COMPUTATIONAL MODELING OF BENZYL ALCOHOL OXIDATION COUPLED WITH
HYDROGEN PRODUCTION IN A PHOTOELECTROCHEMICAL REACTOR

Miss Thorfhan Hanamorn

จุฬาลงกรณ์มหาวิทยาลัย
CHULALONGKORN UNIVERSITY

A Thesis Submitted in Partial Fulfillment of the Requirements
for the Degree of Master of Engineering in Chemical Engineering
Department of Chemical Engineering
FACULTY OF ENGINEERING
Chulalongkorn University
Academic Year 2022
Copyright of Chulalongkorn University

แบบจำลองเชิงคำนวณของปฏิกิริยาออกซิเดชันของเบนซิลแอลกอฮอล์ควบคู่กับการผลิตไฮโดรเจนใน
เครื่องปฏิกรณ์ไฟฟ้าเคมีแบบใช้แสง

น.ส.ทอฝัน หาญอมร

วิทยานิพนธ์นี้เป็นส่วนหนึ่งของการศึกษาตามหลักสูตรปริญญาวิศวกรรมศาสตรมหาบัณฑิต
สาขาวิชาวิศวกรรมเคมี ภาควิชาวิศวกรรมเคมี
คณะวิศวกรรมศาสตร์ จุฬาลงกรณ์มหาวิทยาลัย
ปีการศึกษา 2565
ลิขสิทธิ์ของจุฬาลงกรณ์มหาวิทยาลัย

Thesis Title	COMPUTATIONAL MODELING OF BENZYL ALCOHOL OXIDATION COUPLED WITH HYDROGEN PRODUCTION IN A PHOTOELECTROCHEMICAL REACTOR
By	Miss Thorfhan Hanamorn
Field of Study	Chemical Engineering
Thesis Advisor	Assistant Professor Paravee Vas-Umnuay, Ph.D.

Accepted by the FACULTY OF ENGINEERING, Chulalongkorn University in Partial Fulfillment of the Requirement for the Master of Engineering

.... Dean of the FACULTY OF ENGINEERING

(Professor SUPOT TEACHAVORASINSKUN, D.Eng.)

THESIS COMMITTEE

.... Chairman

(Associate Professor Supareak Praserthdam, Ph.D.)

.... Thesis Advisor

(Assistant Professor Paravee Vas-Umnuay, Ph.D.)

.... Examiner

(Assistant Professor Palang Bumroongsakulsawat, Ph.D.)

.... External Examiner

(Assistant Professor Weekit Sirisaksoontorn, Ph.D.)

ทอฝัน หาญอมร : แบบจำลองเชิงคำนวณของปฏิกิริยาออกซิเดชันของเบนซิลแอลกอฮอล์ควบคู่กับการผลิตไฮโดรเจนในเครื่องปฏิกรณ์ไฟฟ้าเคมีแบบใช้แสง . (COMPUTATIONAL MODELING OF BENZYL ALCOHOL OXIDATION COUPLED WITH HYDROGEN PRODUCTION IN A PHOTOELECTROCHEMICAL REACTOR) อ.ที่ปรึกษาหลัก : ผศ. ดร. ปารวี วาศน์อำนวย

ในเซลล์ไฟฟ้าเคมีแบบใช้แสง (Photoelectrochemical cell) การผลิตไฮโดรเจนที่ขั้วแคโทดต้องควบคู่ไปกับปฏิกิริยาออกซิเดชันที่ขั้วแอโนด การออกซิเดชันเฉพาะของเบนซิลแอลกอฮอล์เป็นเบนซาลดีไฮด์เป็นอีกทางเลือกหนึ่งที่น่าสนใจเนื่องจากมีศักย์ไฟฟ้าเกิน(Overpotential)ที่ต่ำกว่าปฏิกิริยา Oxygen Evolution Reaction (OER) ในงานนี้ ได้ทำการศึกษาการจำลองการออกซิเดชันเฉพาะของเบนซิลแอลกอฮอล์เป็นเบนซาลดีไฮด์ที่จับคู่กับการผลิตไฮโดรเจนเครื่องปฏิกรณ์ไฟฟ้าเคมีแบบใช้แสงแบบ 2 มิติ โดยใช้ COMSOL Multiphysics (5.6) การจำลองการขนส่งประจุและจลนพลศาสตร์ไฟฟ้าเคมีใช้สมการของ Nernst Planck และ Butler Volmer ตามลำดับ ผลการวิจัยพบว่าความเข้มข้นของไฮโดรเจนและเบนซาลดีไฮด์บนพื้นผิวอิเล็กโทรดเพิ่มขึ้นตามทิศทางการไหลของอิเล็กโทรไลต์ที่ขึ้นไปที่ส่วนท้ายของเครื่องปฏิกรณ์ นอกจากนี้ การสะสมของไฮโดรเจนและความเข้มข้นของเบนซาลดีไฮด์บนพื้นผิวอิเล็กโทรดลดลงอย่างมีนัยสำคัญเมื่อความเร็วของอิเล็กโทรไลต์เพิ่มขึ้นเนื่องจากแรงเฉือนที่สูงขึ้น นอกจากนี้ แบบจำลองเครื่องปฏิกรณ์ไฟฟ้าเคมีแบบใช้แสงแบบ 3 มิติยังถูกจำลองเพื่อให้ได้การออกแบบและการวางแนวที่เหมาะสมที่สุด ผลการจำลองสำหรับแบบจำลองเครื่องปฏิกรณ์ไฟฟ้าเคมีแบบใช้แสงทั้งหมดแสดงให้เห็นถึงการไหลที่เป็นการเคลื่อนที่เชิงเส้นแบบสม่ำเสมอซึ่งเป็นลักษณะเฉพาะของการไหลแบบลามินาร์ โมเดลเครื่องปฏิกรณ์ไฟฟ้าเคมีแบบใช้แสงที่มีการวางแนวในแนวนอนได้แสดงให้เห็นตัวเลือกที่ดีที่สุดสำหรับการผลิต เนื่องจากแรงดันตกคร่อมที่ต่ำกว่าเมื่อเปรียบเทียบกับแบบที่มีการวางแนวในแนวตั้ง

สาขาวิชา	วิศวกรรมเคมี	ลายมือชื่อนิสิต ....
ปีการศึกษา	2565	ลายมือชื่อ อ.ที่ปรึกษาหลัก ....

6370111021 : MAJOR CHEMICAL ENGINEERING

KEYWORD: Photoelectrochemical reactor, CFD simulation, Selective alcohol oxidation, Benzaldehyde, Hydrogen production

Thorfhan Hanamorn : COMPUTATIONAL MODELING OF BENZYL ALCOHOL OXIDATION COUPLED WITH HYDROGEN PRODUCTION IN A PHOTOELECTROCHEMICAL REACTOR. Advisor: Asst. Prof. Paravee Vas-Umnuay, Ph.D.

In photoelectrochemical (PEC) cells, hydrogen production at the cathode must be coupled with the oxidation reaction at the anode. Selective oxidation of benzyl alcohol into benzaldehyde is an attractive alternative pathway due to its lower overpotential than the traditional oxygen evolution reaction (OER). In this work, simulation of selective oxidation of benzyl alcohol into benzaldehyde paired with hydrogen production in 2 chambers of 2-dimensional PEC reactor was studied using COMSOL Multiphysics (5.6). Charge transport and electrochemical kinetics were simulated using Nernst Planck's and Butler Volmer's equations, respectively. The results have showed that hydrogen and benzaldehyde concentrations on electrode surfaces increased with the direction of electrolyte flow to the posterior end of the reactor. Moreover, the accumulation of hydrogen and benzaldehyde concentration on electrode surfaces decreased significantly with an increase of electrolyte velocity due to the higher shear force. In addition, the 3-dimensional PEC reactor model was also simulated to obtain the optimal design with the best orientation. The results for all PEC reactor model show streamline as a uniform linear motion which is a characterization of a laminar flow. The horizontal PEC reactor model has shown the best choice for fabrication because of lower pressure drop compared to that of the one with vertical orientation.

Field of Study:	Chemical Engineering	Student's Signature	....
Academic Year:	2022	Advisor's Signature	....

ACKNOWLEDGEMENTS

จุฬาลงกรณ์มหาวิทยาลัย

CHULALONGKORN UNIVERSITY

TABLE OF CONTENTS

Page

จุฬาลงกรณ์มหาวิทยาลัย
CHULALONGKORN UNIVERSITY

LIST OF TABLES

LIST OF FIGURES

CHAPTER 1

INTRODUCTION

1.1 Background

Biomass is one type of renewable energy source which can be converted into valuable products. The conversion process of biomass has become a promising pathway to increase the energy production. In the past, energy from biomass was generally obtained from the combustion process that released pollutants to the environment [1]. In addition, other methods of biomass conversion to fuels consist of gasification, pyrolysis, and hydrolysis. Even though these methods can give high-value products, such as synthesis gas and methanol, they require high temperature and pressure for operation [2].

Photoelectrochemical (PEC) cell is a new advanced oxidation technology that was first reported in 1972. Among applications that use PEC cells, the water-splitting process has been vastly studied. In general, their applications have been widely reported in many fuels production fields such as carbon dioxide conversion and degradation of pollutants due to their advantages such as mild and economical operating conditions, and environmentally friendly [3]. Normally, water splitting in PEC cells consists of hydrogen production at the cathode paired with oxygen evolution reaction (OER) at the anode. Water is split into hydrogen and oxygen when a semiconductor material that is used as a photoanode is illuminated by a light source. The electrons in the valence band get energized and move to the conduction band creating electron-hole pairs. These electron-hole pairs are separated in the opposite directions to the electrode surface. Holes in the valence band oxidize the water molecule into oxygen and hydrogen ions (protons) [4]. However, large overpotential is required to drive OER. This results in an increase in applied voltage to the cells [5]. Therefore, many reactions have been investigated to find the alternative anodic reaction that can be paired with hydrogen production. The oxidation reaction of biomass alcohol into its corresponding aldehydes is another attractive pathway due to its lower overpotential than OER. In the last few years, a lot of PEC cell research have been studied to improve electrode materials to

increase the stability and efficiency, and modeling of practical PEC reactor was also studied.

In this work, the photoelectrochemical cell consisting of titanium dioxide (TiO_2) used to oxidize benzyl alcohol in the anodic chamber, and a platinum plate (Pt) used as an electrode in the cathodic chamber to produce hydrogen. Benzyl alcohol was selected as the model of biomass alcohol. This work aims to simulate the PEC reactor model that combines selective oxidation reaction at the anode with the hydrogen production at the cathode using COMSOL Multiphysics (5.6) to achieve high selectivity and high yield of benzaldehyde and hydrogen. To elaborate the process, the mechanism of selective benzyl alcohol oxidation and hydrogen production was also investigated.

1.2 Objectives

1. To simulate a photoelectrochemical reactor model for benzyl alcohol oxidation paired with hydrogen production.

2. To study the effects of benzyl alcohol flow rate on benzaldehyde concentration in the photoelectrochemical reactor model.

1.3 Scope of Research

Photoelectrochemical reactor for benzyl alcohol oxidation paired with hydrogen production was simulated as a backside illumination flat plate reactor in a 2-dimensional and 3-dimensional model by using COMSOL Multiphysics (5.6). The model was assumed as incompressible fluid. The flow rate of anolyte and catholyte were varied in laminar flow regimes (Re < 2300).

1.4 Expected Benefits

1. Photoelectrochemical reactor model for benzyl alcohol oxidation paired with hydrogen production is developed.

2. The effects of benzyl alcohol flow rate in the photoelectrochemical reactor model is studied.

CHAPTER 2

THEORETICAL BACKGROUND AND LITERATURE REVIEW

To study benzyl alcohol oxidation into benzaldehyde paired with hydrogen production in the photoelectrochemical reactor, the related theory and literature review are as follows:

2.1 Benzaldehyde

Benzaldehyde is the simplest and most important aromatic aldehyde. It can be found in form of combined and uncombined forms in many plants. The well-known natural source of benzaldehyde is amygdalin, which exists in a combined form of glycoside, and is present in bitter almonds. The bitter almond odor is caused by a small amount of free benzaldehyde, which is produced by the hydrolysis of amygdalin. According to its existence in bitter almonds, the aldehyde was referred to as "bitter almond oil" [6].

2.1.1 Applications of benzaldehyde

Benzaldehyde is a starting material for odorants and flavors manufacture. It is incorporated directly in perfumes, foods, drinks, and other products. In addition, it is almost used in the production of derivatives that are also used in the perfume and flavor industries. Examples of benzaldehyde derivatives are cinnamaldehyde, cinnamaldehyde dimethyl acetal, and benzyl benzoate. Another application of benzaldehyde is triphenylmethane dyes production. In the pharmaceutical industry, benzaldehyde is used as an intermediate in the production of chloramphenicol, ephedrine, ampicillin, and other products. Other important chemical intermediates obtained from benzaldehyde are benzoin, benzylamine, and mandelic acid. In addition, benzaldehyde is used as a corrosion inhibitor in photochemistry [6].

2.1.2 Benzaldehyde production

Benzaldehyde can be produced from many pathways depending on different substrates such as hydrolysis of benzal chloride, oxidation of toluene, or oxidation of benzyl alcohol.

1. Hydrolysis of benzal chloride

The hydrolysis of benzal chloride is the oldest process to produce benzaldehyde. It can be carried out in both alkaline and in an acidic medium [6].
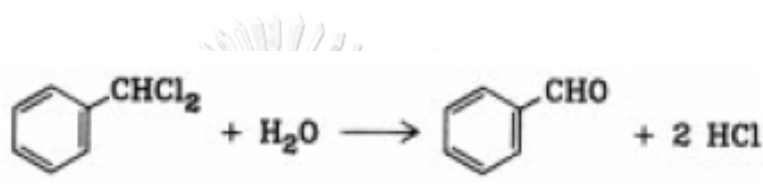
Figure 1. The hydrolysis reaction of benzal chloride to benzaldehyde. [6]

Hydrolysis under basic conditions can be carried out with calcium hydroxide, calcium carbonate, sodium hydrogen carbonate, or sodium carbonate. Excess of the alkaline medium increases the probability of side reactions. Sodium carbonate is widely used as an alkaline medium. According to the process, benzal chloride is saponified with an excess of 15% sodium carbonate solution at 138 °C. When the saponification is complete, benzaldehyde is isolated from the mixture by steam distillation and distilled at 0.02 - 0.03 bar. The chlorine content of the distilled product is less than 0.01 % [6].
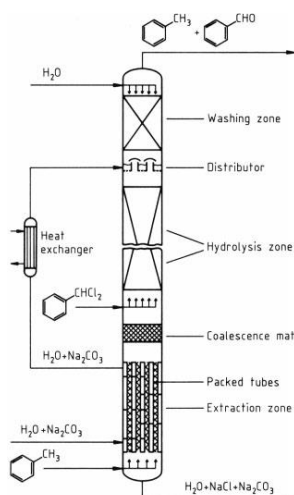
Figure 2. Hydrolysis of benzal chloride to benzaldehyde in a flow-through reactor. [6]

In a continuous process as shown in figure 2, benzal chloride and the alkaline hydrolyzing agent are reacted as countercurrents in a flow reactor with the existence of an organic solvent (e.g., toluene, xylene) under the temperature of 125 – 145 °C and a pressure of 12 – 18 bar. In the extraction zone, the dissolved aldehyde is extracted from the alkaline phase using an organic solvent flowing from the bottom. In the washing zone, Water is used to washes the crude benzaldehyde from a solution. The wash water and extract are returned to the hydrolysis zone to recover benzaldehyde [6].

2. Oxidation of toluene

The oxidation of toluene with oxygen to produce benzaldehyde is carried out in both the gas phase and the liquid phase. Benzaldehyde can be oxidized to benzoic acid and other products. Therefore, conditions must be controlled carefully to prevent side reactions [6].
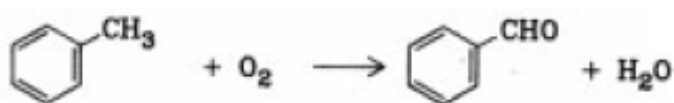
Figure 3. The Oxidation reaction of toluene to benzaldehyde. [6]

In the gas phase, the oxidation of toluene is carried out by feeding toluene vapor with oxygen through a catalyst bed in a fluidized-bed reactor at a temperature of 250 – 650 °C. Because the reaction is highly exothermic, an effective cooling system is necessary. It is recommended to dilute toluene vapor and oxygen-containing gas mixtures with non-reactive gases such as water vapor, nitrogen, or carbon dioxide. The oxides of the elements of Groups V and VI are used as catalysts, sometimes with other oxides. These oxide catalysts contain molybdenum and at least one additional element of iron, nickel, or cobalt [6].

3. Oxidation of benzyl alcohol
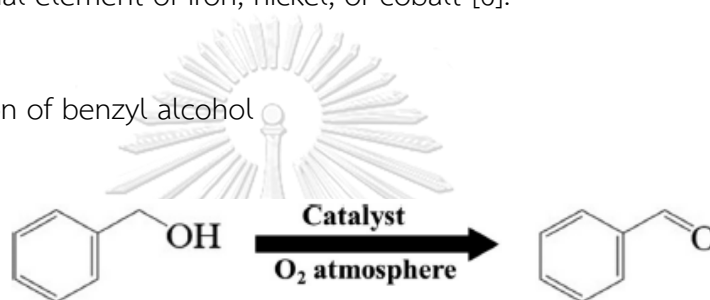
Figure 4. The Oxidation reaction of benzyl alcohol to benzaldehyde. [7]

The oxidation of benzyl alcohol has been reported in different oxidation pathways that form benzaldehyde and benzoic acid, toluene depending on the catalyst used. The operating condition of benzyl alcohol was reported in many pathways depending on catalyst and process use. The selective oxidation of benzyl alcohol to benzaldehyde is an important commercial process, as high-quality high-grade benzaldehyde is important in perfumery, pharmaceutical, and agrochemicals industries [8].

The oxidation of benzyl alcohol to benzaldehyde was reported in many processes such as catalytic oxidation, photocatalytic oxidation, and photo electrocatalytic oxidation.

2.2 Hydrogen

Hydrogen is a clean energy carrier, not an energy source, that can be an important role in global energy production. Hydrogen from renewable sources is a zero-carbon production pathway [9].

2.2.1 Applications of hydrogen

Most of the hydrogen today is produced and used in industry. From figure 5, two-thirds of the use of hydrogen is used in ammonia production and oil refining. At petroleum refining, hydrogen is added to heavy oil for transport fuel production [9].
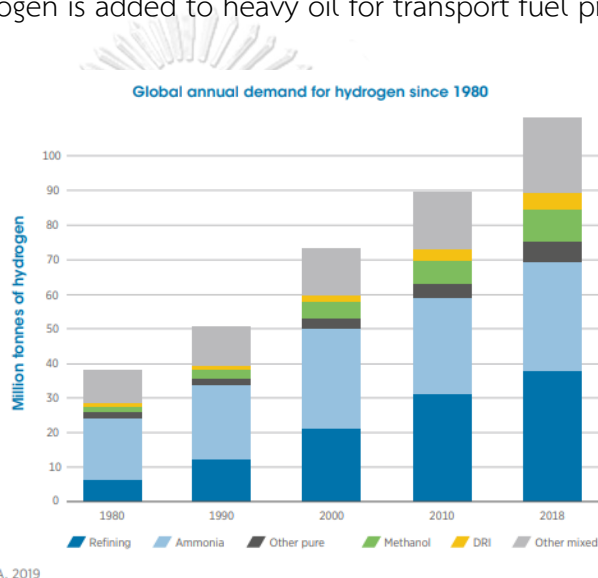
Figure 5. Global annual hydrogen demand from 1980 to 2018. [9]

2.2.2 Hydrogen production

Hydrogen can be produced from many different resources including fossil fuels, natural gas and coal, biomass, and crops, or using nuclear energy and renewable energy sources, such as wind, solar, geothermal, and hydroelectric power to split water. Hydrogen production can be categorized into 3 main processes [10].

1. Thermal process

In the thermal process, hydrogen sources such as natural gas, coal, and biomass are heated to high temperature to obtain products[10]. It consists of natural gas conversion, gasification of biomass, and high-temperature water splitting.

- **Natural gas reforming**

Hydrogen can be produced from natural gas by 3 different chemical processes:

1. Steam reforming (steam methane reforming – SMR).

2. Partial oxidation (POX).

3. Autothermal reforming (ATR).

Steam reforming is the endothermic reaction including methane conversion with water vapor into carbon monoxide and hydrogen as equation (1). The supplied heat is from the combustion of partial methane in feed-gas. The process usually operates at temperatures of 700 - 850 ℃ and pressures of 3 - 25 bar. The gas product contains approximately 12 % CO, which can be converted to CO_2 and H_2 through the water-gas shift reaction as the following equation (2). [11]

$$CH_4 + H_2O + heat \longrightarrow CO + 3H_2 \tag{1}$$
$$CO + H_2O \longrightarrow CO_2 + H_2 + heat \tag{2}$$
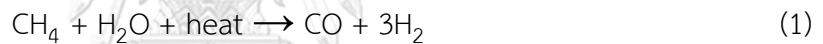
Partial oxidation of natural gas is a process that produces hydrogen through the combustion of methane with partial oxygen to obtain carbon monoxide and hydrogen as shown in equation (3). Because this process is an exothermic reaction, any external heating of the reactor is not required. The CO conversion is converted to H_2 as described in equation (2). [11]

$$CH_4 + \frac{1}{2}O_2 \longrightarrow CO + 2H_2 + heat \tag{3}$$
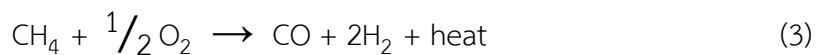
Autothermal reforming is a combination of steam reforming (1) and partial oxidation (3). The total reaction is exothermic. The temperature at the outlet of the reactor is 950 - 1100 ℃, and the pressure can be up to 100 bar [11]. The CO conversion is also converted to H_2 through the water-gas shift reaction (2).

- **Gasification**

Hydrogen can be produced from coal through different gasification processes (e.g., fixed bed and fluidized bed or entrained flow). In general, high-temperature entrained flow processes are preferred to increase carbon conversion to gas, thus the formation of char, tars, and phenols are avoided.[12] A reaction for the process is described in equation (4). [11]

$$C_{(s)} + H_2O + heat \longrightarrow CO + H_2 \qquad (4)$$
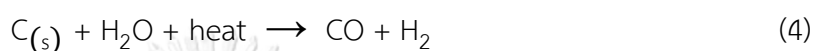
Because this reaction is endothermic, supplied heat is needed. The CO is converted to CO_2 and H_2 through the water-gas shift reaction, described in equation (2). Hydrogen production from coal is growing commercially, but it is more complicated than the production from natural gas. [11]

- **High-Temperature water splitting**

In traditional, high temperature water splitting occurs at about 3000 °C. At this temperature, 10% of the water is usually decomposed and the remaining 90% can be recycled. To reduce the temperature, other processes for high temperature water splitting have been suggested [11].

Thermochemical water splitting is the conversion of water into hydrogen and oxygen by a series of thermal-driven chemical reactions. An example of a thermochemical process is the iodine/sulfur cycle, shown in equations (5), (6), and (7) and figure 6 For this process, the research and development needs are to capture the thermally split H_2, to avoid side reactions, and to eliminate the use of toxic substances [11].

(850 °C): $\qquad H_2SO_4 \longrightarrow SO_2 + H_2O + {}^1\!/_2\, O_2$ $\qquad$ (5)

(120 °C): $\qquad I_2 + SO_2 + 2H_2O \longrightarrow H_2SO_4 + 2HI$ $\qquad$ (6)

(450 °C): $\qquad 2HI \longrightarrow I_2 + H_2$ $\qquad$ (7)

Over-all reaction: $\qquad H_2O \longrightarrow H_2 + {}^1\!/_2\, O_2$
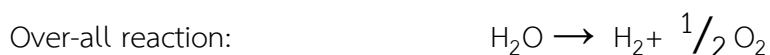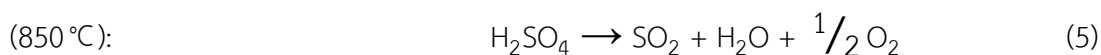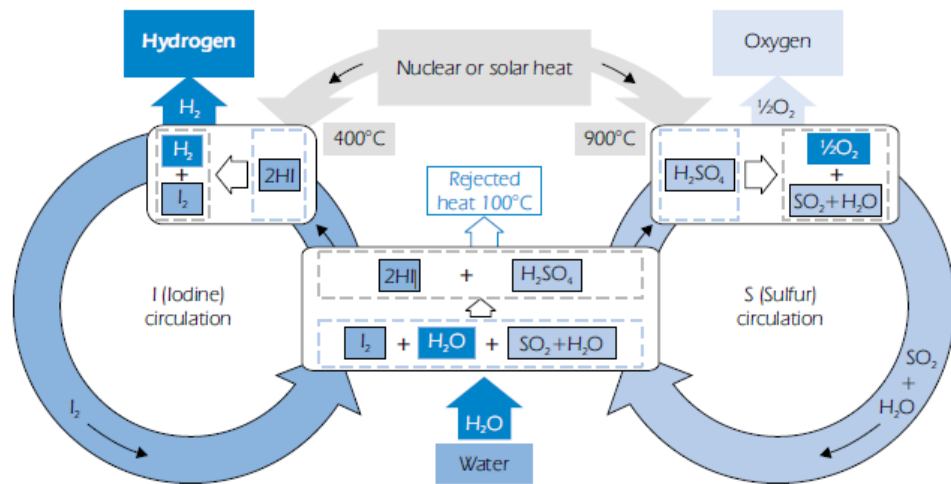
Figure 6. Principle of iodine/sulfur thermochemical process.[11]

2. Electrolytic Process

Water electrolysis uses electricity to split water into hydrogen and oxygen. Hydrogen production by the electrolysis process has zero greenhouse gas emissions, depending on the source of the electricity. The electrolysis process is less efficient than the direct chemical pathway. However, there is almost no pollution or toxic by-products if electricity is generated using renewable energy [10].

In equation (8), The total energy required for electrolysis of water increases slightly with temperature, while the required electrical energy decreases. Therefore, a high-temperature electrolysis process is more suitable when applied heat is waste heat from other processes [11].

$$H_2O + electricity \longrightarrow H_2 + {}^1\!/_2\, O_2 \tag{8}$$
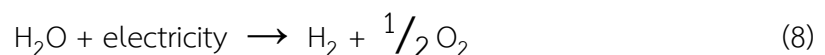
- **Alkaline electrolysis**

Alkaline electrolyzers use an aqueous KOH solution as an electrolyte that circulates through the electrolytic cells. This process is suitable for stationary

applications and available at operating pressures up to 25 bar [11]. Reactions inside the alkaline cell are following:

Electrolyte: $\qquad$ $4H_2O \longrightarrow 4H^+ + 4OH^-$ $\qquad$ (9)

Cathode: $\qquad$ $4H^+ + 4e^- \longrightarrow 2H_2$ $\qquad$ (10)

Anode: $\qquad$ $4OH^- \longrightarrow O_2 + 2H_2O + 4e^-$ $\qquad$ (11)

Overall reaction: $\qquad$ $2H_2O \longrightarrow O_2 + 2H_2$ $\qquad$ (12)
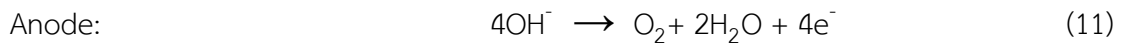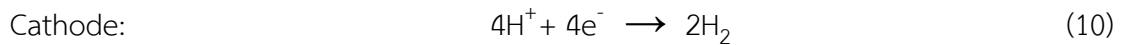
Commercial alkaline electrolyzers normally consist of several electrolytic cells arranged in a cell stack. The main components of alkaline electrolyzers are shown in figure 7.
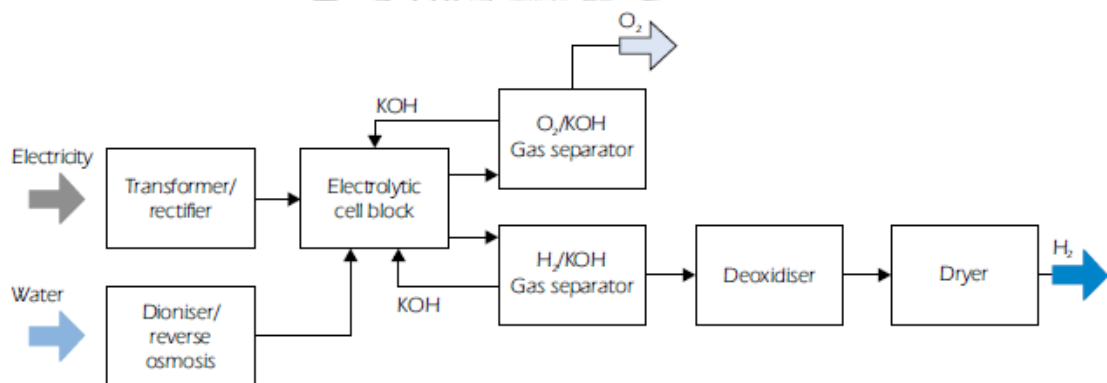
Figure 7. Process diagram of alkaline electrolysis. [11]

- **Polymer electrolyte membrane (PEM) electrolysis**

The PEM electrolyzers do not require a liquid electrolyte which greatly simplifies the design. The electrolyte is an acidic polymer membrane. PEM electrolyzers can be operated for pressures up to 100 bar and are suitable for both stationary and mobile applications. The main disadvantage of PEM is the limited-service life of the membrane. The major advantages of PEM over alkaline electrolyzers are the higher turndown ratio (operating ratio of part load to full load.), The system is more secure due to the absence of KOH electrolytes, and a more compact design due to higher density, and operating pressures [11]. The principle of PEM electrolysis is presented in equations (13) and (14).

Anode: $$H_2O \longrightarrow \tfrac{1}{2}O_2 + 2H^+ + 2e^- \tag{13}$$

Cathode: $$2H^+ + 2e^- \longrightarrow H_2 \tag{14}$$
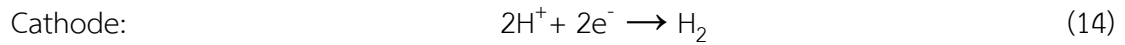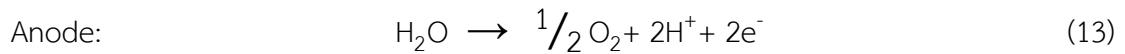
3. Photolytic Process

Photolytic processes use energy from light sources to split water into hydrogen and oxygen. Currently, these processes offer the long-term potential for sustainable hydrogen production with low environmental pollutants [11].

- **Photoelectrochemical water splitting**

Photovoltaic (PV) systems connected to the electrolyzer are flexible because the output can be electricity from the PV cells or hydrogen from the electrolyzer. Direct photoelectrolysis represents an advanced alternative to PV electrolyte systems by combining the two processes in one device. This principle is shown in figure 8 Water photoelectrolysis is a process that uses light to directly split water into hydrogen and oxygen [11].
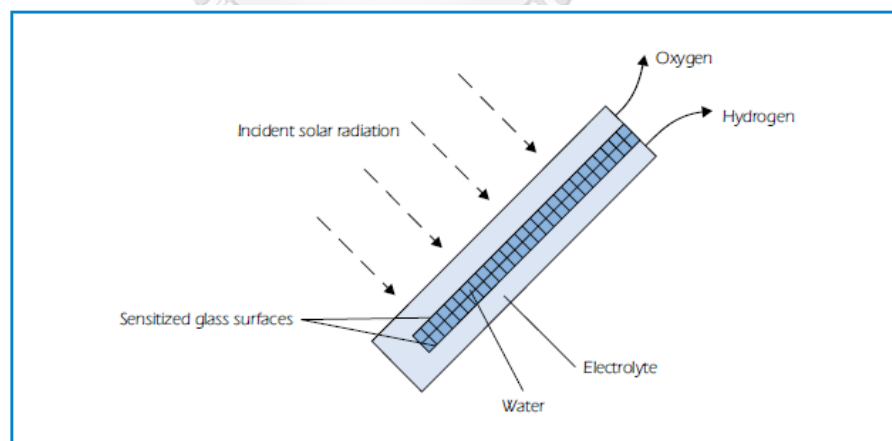
Source: Hydrogen Solar Production Company Inc.

Figure 8. Principle of the photo-electrolytic cell. [11]

- **Photobiological water splitting**

Photobiological hydrogen production consists of two main steps: photosynthesis and hydrogen production in green algae and cyanobacteria. Long-term basic and applied research is needed in this field. if successful It could be a long-term solution for renewable hydrogen production. Metabolic and genetic engineering should be used to develop the process for larger bioreactors [11]. Photosynthesis and hydrogen production reaction is shown in equations (15) and (16), respectively.

Photosynthesis: $2H_2O \longrightarrow 4H^+ + 4e^- + O_2$ (15)

Hydrogen production: $4H^+ + 4e^- \longrightarrow 2H_2$ (16)
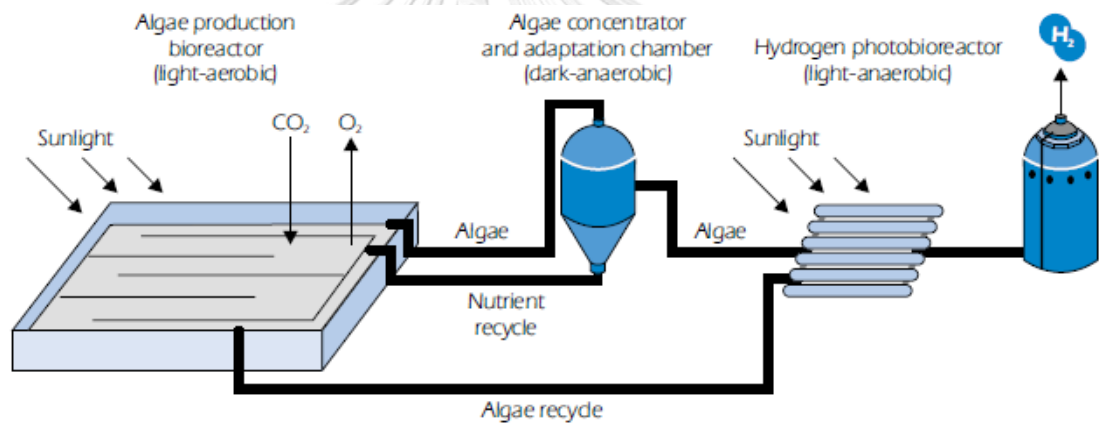
Figure 9. Principle of photo-biological hydrogen production. [11]

2.3 Photoelectrochemical cells

2.3.1 Principle of Photoelectrochemical cells
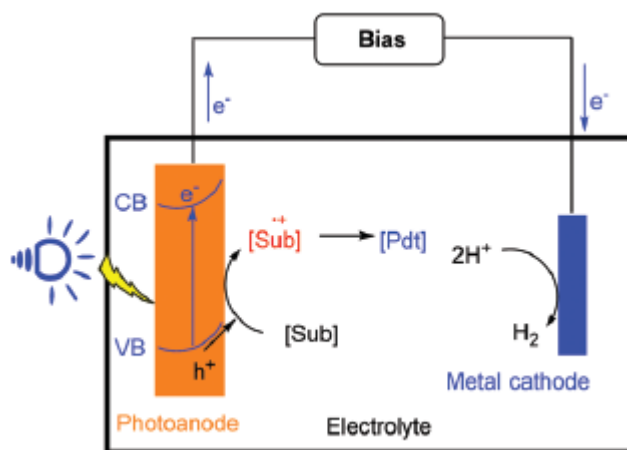
Figure 10. Principle of the photoelectrochemical cell. [3]

Figure 10 shows the principle of photoelectrochemical cells. A semiconductor is used as a photoanode that converts photons to electron-hole pairs when it is illuminated. These electrons and holes are separated due to the existence of an electric field inside the semiconductor. The photogenerated electrons move toward the conducting band and go to the metal counter electrode via an external wire. The electrons are combined with protons to form hydrogen gas at the cathode. The photogenerated holes move to the semiconductor/electrolyte interface, to oxidize substrate into product [12].

2.3.2 Types of photoelectrochemical reactor

1. Based on a fluidized bed of semiconductor particle

Photocatalytic reactors using particulate semiconductors are widely used for the oxidation of dissolved organic compounds in aqueous media. Suspended semiconductor particles are used in cylindrical reactors. to retain the particles in the suspension, the flow rate should be uniform. PEC reactors have been developed based on a fluidized bed of semiconductor particles, where fluid flow suspends the particles which can provide light both internally using artificial light or from outside using solar radiation, as shown in figure 11, the rate of reaction depends on the active electrode area, mass transfer rates due to the fluid flow. However, products of both reduction and oxidation reactions are produced without separation and reverse reaction can occur. For safety and efficient operation, product separation is required [13].
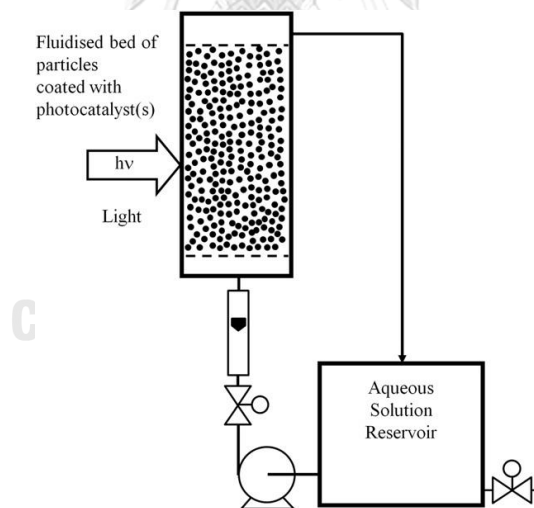
Figure 11. The concept for the PEC reactor is based on a fluidized bed of semiconductor particles.[13]

2. Based on a modified optical fiber
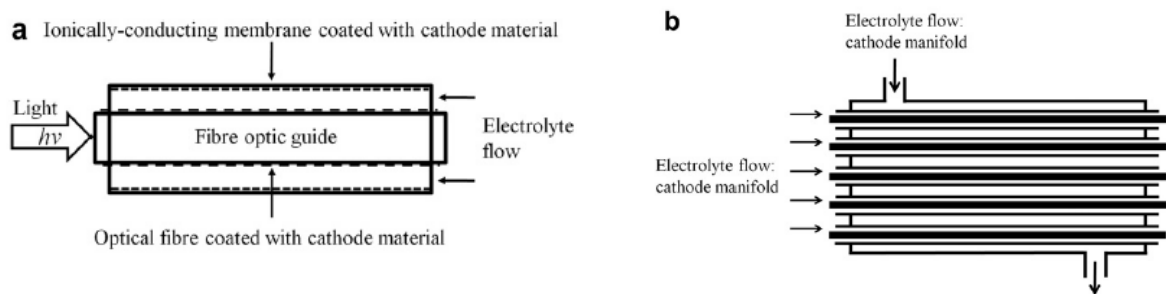
Figure 12. The concept for the PEC reactor is based on a modified optical fiber.[13]

In figure 12, the PEC reactor which is based on a modified optical fiber is shown. A single photoactive optical fiber element is shown in figure 12(a) which consists of a semiconductor-coated optical fiber as a photoanode is enclosed in a sheath of ionic conductive polymer. The cathode may be an additional tube of a suitable metal (nickel), or the metal cathode may be constructed on the ion-conductive polymer itself. The metal must be porous to allow the electrolyte contact with the membrane. but still provides electrical continuity [13].

The PEC reactor scale-up was done by bundling optical fiber together into a manifold arrangement as shown in figure 12(b). This arrangement was created to separate the product from the cathode and anode sides and have good light access along with the optical fiber. However, the axial current was accumulated along with thin layers of semiconductor-coated optical fiber due to low conductivity. This will result in non-uniform potential distribution and lengthwise scale-up may be limited and results in the benefit of illumination via optical fibers [13].

3. Based on a flat plate reactor
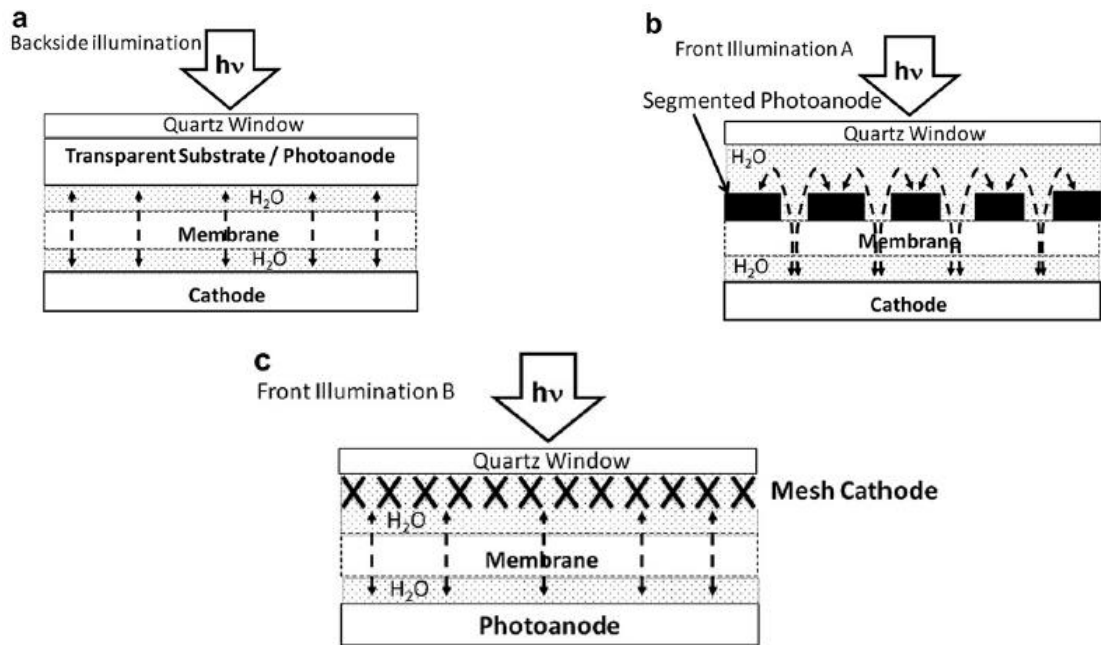
Figure 13. The concept for the PEC reactor is based on a flat plate reactor. [13]

The PEC reactor which is based on planar or parallel electrodes is the simplest concept. This concept is consisting of cathode and anode facing each other, the membrane between them, and electrolytes. A window at the side or top of the reactor allows light to illuminate the photoanode. A simple flat photoelectrode is required usually as a thin film of semiconductor on a conducting substrate such as a transparent conductor, e.g., ITO or F-TO on glass [13].

From figure 13, The PEC reactor chamber is divided into two parts by an ion-exchange membrane to separate products from anode and cathode. Figure 13(a) shows the back-illumination through the photoanode which can act as a window and solar absorber. In this case, current flows directly from anode to cathode and has a uniform potential distribution [13].

The photoanode which is fabricated on a non-light transmitting substrate allows only front illumination, as shown in figure 13(b) and (c). The photoanode faces away from the cathode presented in figure 13(b). Due to this configuration, a current

distribution problem may occur. Therefore, the photoanode is constructed as a segmented form to decreases the effect of non-uniform current distribution but increase the complexity and cost of reactor fabrication. To resolve the non-uniform current distribution problem, a semitransparent (mesh) cathode is required that is placed above the photoanode, as shown in figure 13(c). [13]

2.4 Benzyl alcohol oxidation coupled with hydrogen production in PEC cells
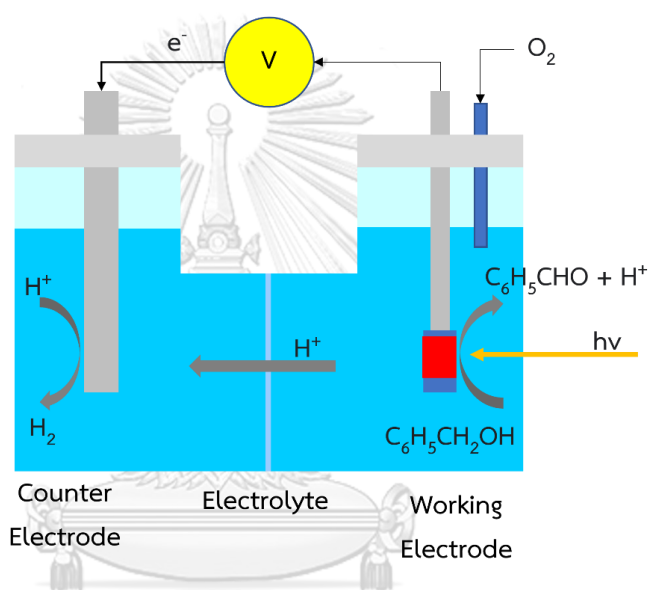
Figure 14. Benzyl alcohol oxidation coupled with hydrogen production in photoelectrochemical cells. [1]

From figure 14, on the anode side, when a semiconductor that is used as a photoanode is irradiated by solar light, the photoanode generates electron-hole pairs. The benzyl alcohol is adsorbed on the surface of the photoanode, and it can be oxidized by photogenerated holes and react with an oxygen molecule to generate benzaldehyde and hydrogen ion (proton). The photogenerated electron will be transferred to the cathodic chamber via external wire to combine with protons that pass-through ion-exchange membrane to generate hydrogen molecule [1]. Reaction in anode and cathode side are following equation (20) to (22).

Anode:
$$semiconductor \xrightarrow{h\upsilon} h^+ + e^- \qquad (20)$$

$$C_6H_5CH_2OH + 2h^+ \xrightarrow{O_2} C_6H_5CHO + 2H^+ \qquad (21)$$

Cathode:
$$2H^+ + 2e^- \longrightarrow H_2 \qquad (22)$$

Overall reaction:
$$C_6H_5CH_2OH \xrightarrow{h\upsilon, \; O_2} C_6H_5CHO + H_2 \qquad (23)$$
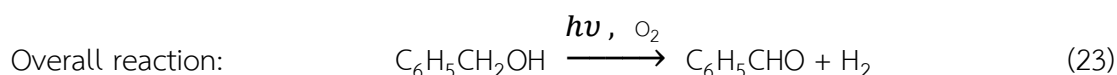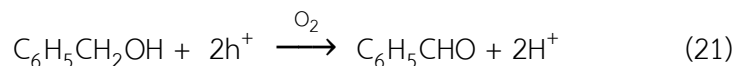
2.5 Literature Review

S. Schünemann et al. synthesized $CsPbBr_3/TiO_2$ photocatalysts at low temperatures via the wet impregnation method to enhance the benzyl alcohol oxidation activity with a selectivity of < 99 % into benzaldehyde at a conversion of 50 % in cyclohexane. Action spectra and ESR studies show that the photogenerated electrons formed under visible light illumination inside $CsPbBr_3$ were moved to the conduction band of TiO_2 where the oxygen molecule was reduced to superoxide ion. Post-characterization via XRD, XPS, UV-vis spectroscopy, and HAADF-STEM studies showed good stability of the all-inorganic halide perovskites in both morphology and crystal structure [14].

C. Xu et al. successfully synthesized the Ti_3C_2/TiO_2 photocatalysts via a hydrothermal method with a mild chemical process. Ti_3C_2/TiO_2 photocatalysts showed excellent selectivity for the oxidation of benzyl alcohol into benzaldehyde under visible light. The Ti_3C_2/TiO_2-0.7 exhibits 92% benzyl alcohol conversion and almost 99% benzaldehyde selectivity is observed. The photocatalytic activity of Ti_3C_2/TiO_2-0.7 photocatalyst is caused to the addition of Ti_3C_2, which results in the narrowed energy band gap by adjusting the position of the conduction band (CB) and valence band (VB) of TiO_2 and the enhanced light-harvesting ability. In their design, a Schottky barrier is exhibited between Ti_3C_2 and TiO_2 nanowires to decrease the recombination probability of electron-hole pairs [15].

Z. Wu et al. combined the selective oxidation of reaction of biomass alcohol at the anode with hydrogen production at the cathode in PEC cell double chamber batch reactor using Au/TiO_2 nanotubes photonic crystals (NTPC) and C/Cu_2O Nanowires arrays (NWAs) as photoanode and photocathode respectively. Benzyl alcohol was used as a biomass alcohol model and oxidized into its corresponding aldehyde, benzaldehyde. 0.1 M sodium sulfate (Na_2SO_4) was used as the electrolyte in both anodic and cathodic sides. The conversion of benzyl alcohol was 84.68% and the selectivity can reach more than 99%. The hydrogen production at the cathode can reach 143.83 μmol/cm^2. This PEC cell generated a current density of more than 0.5 mA/cm^2 [1].

Similar to previous work, Z. Zhou, Y. et al. also combined benzyl alcohol oxidation with hydrogen production in PEC cell double chamber batch reactor. It consists of a bismuth molybdenum oxide doped TiO_2 nanotube arrays (Bi_2MoO_6@TiO_2 NTA) photoanode and a photocathode constructed from the carbon-doped Cu_2O nanowires (C/Cu_2O NW). 0.1 M Na_2SO_4 was used as the electrolyte in both anodic and cathodic sides. The electrons generated during the oxidation reaction were utilized as the source for hydrogen production. The amount of hydrogen concentration was 5.5 times higher than when OER was used on the anode side. The efficiency of hydrogen production was 85 % [16].

F. Farivar studied and improved PEC reactor performance using COMSOL Multiphysics software. The PEC reactor was simulated in the oval-shaped chamber because of minimum dead zones and uniform electrolyte flow profile. Additionally, the potential drop due to resistance of transparent conducting films (TCFs) was improved by adding a golden grid layer on TCFs. Simulation results confirmed that using a thin layer of golden mesh, will increase the conductivity of TCFs. The potential drop across an FTO film decreased from 25% to about 6% [17].

F. N. Njoka et al. investigated the transport phenomena and electrochemical kinetics in the two electrolyte chambers of a 2-dimensional PEC reactor for water splitting reaction using COMSOL Multiphysics software. The ion-exchange membrane is included in the simulations to separate the reaction products from both sides, H_2 and O_2, which will result in product losses and cause danger under normal operations of the PEC reactor. although the dissociation rate of water was low, a positive dissociation and proton movement from the anolyte to the catholyte was observed. The evolution of hydrogen and oxygen from the cathode and anode surfaces was respectively reported. Gas product concentration appeared at the electrode surfaces where the reactions occurred with the high concentration band widening along with the reactor height. The results also showed the ratio of increment in hydrogen concentration ratio was double times of oxygen which mimics the equilibrium of water splitting reaction. Moreover, photocurrent density was also increased by increasing gas production [18].

Table 1. Literature review summary

Authors	Process	Materials	Electrolyte	Results	Light source
S. Schünemann et al. (2018),[14]	Photocatalytic oxidation	$CsPbBr_3/TiO_2$		50% BA conversion 99% BAD selectivity	Visible
C. Xu et al. (2020),[15]		Ti_3C_2/TiO_2		92% BA conversion 99% BAD selectivity	Visible
Z. Wu et al. (2013), [1]	Photoelectrochemical oxidation	Anode: Au/TiO_2 NTPC Cathode: C/Cu_2O NWA	Na_2SO_4	85% BA conversion 99% BAD selectivity 143.83 H_2 μmol/cm^2 Current density 0.5 mA/cm^2	Visible
Z. Zhou, Y. et al. (2020),[16]		Anode: Bi_2MoO_6@TiO_2 NTA Cathode: C/Cu_2O NW	Na_2SO_4	67.4% BA conversion 98% BAD selectivity 114.6 H_2 μmol/cm^2 Current density 0.54 mA/cm^2	Visible
F. Farivar (2016),[17]	Simulation of Water splitting in PEC reactor	Anode: FTO	H_2O	1. improved electrolyte flow to be more uniform by changing PEC configuration from normal rectangular into oval shape. 2. improved potential drop across photoanode by adding golden mesh on FTO.	
F. N. Njoka et al. (2017),[18]		Anode: Fe_2O_3 Cathode: Pt	H_2O	1. water splitting in the flow reactor was investigated. Gas products appear at the surface of both electrodes along the reactor heigh. 2. Hydrogen concentration ratio was twice that of oxygen. 3. An increase in the photocurrent density increased gas product.	

BA: Benzyl alcohol, BAD: Benzaldehyde

CHAPTER 3

METHODOLOGY

3.1 PEC reactor model descriptions
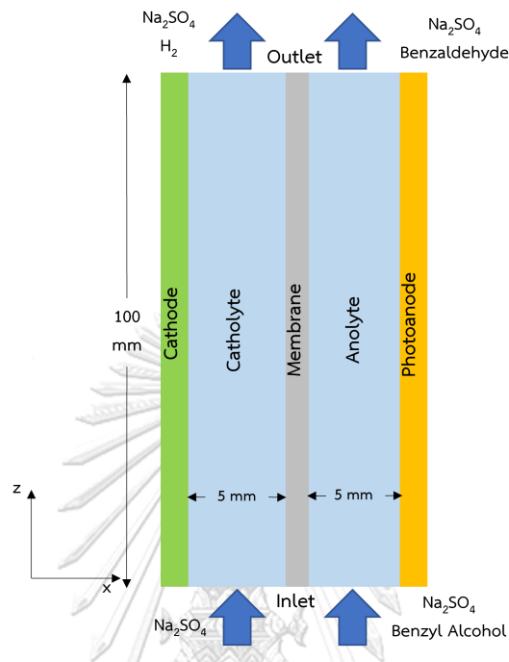
Figure 15. Schematic of cell design for a photoelectrochemical reactor.

Figure 15 shows schematic illustrations of the PEC cell designs that were evaluated for PEC performance. It was simulated in a 2-dimensional(2-D) cross-section model constructed with 5 domains consisting of photoanode and cathode, anolyte and catholyte, and proton-exchange membrane. TiO_2 was used to simulate as a photoanode and Pt as a cathode. The all-domains height was controlled at 100 mm. COMSOL Multiphysics (5.6) with a stationary and time dependent with initialization study were carried out using a finite element numerical simulation model to simulate the behavior of the PEC reactor. In all domains, secondary current distribution (CD) coupled with transport of diluted species was used to analyze electrokinetic in the reactor model but in proton-exchange membrane used secondary current distribution.

0.1M Na_2SO_4 was used as the electrolyte model and fed from the inlets at bottom of the cell in the z-direction. The Reynold number of electrolyte flow was assumed to be in a laminar regime in the range of 0.002 - 0.006 m/s. The oxidation

and reduction reactions took place at the internal surfaces of photoanode and cathode respectively. The concentration of all species was considered for the model. A Danckwert's boundary condition was applied at the inlets to maintain both the reactant flux and the continuity of reactants concentrations. Both ion fluxes and charge transport in the model were estimated using Nernst Plank's equation. The Butler-Volmer's equation was applied on both electrode surfaces to simulate electrode surface reaction with electrode length of 100 mm. The outer cathode surface was grounded, and the outer anode surface was set under a constant photocurrent density as input flux. Modeling parameters used in the simulation are shown in table 3.

Moreover, the configuration and orientation of 3-dimensional (3-D) PEC reactor model were also simulated with the stationary study. The schematic of 3-D PEC reactor is show in figure 16 with the dimension in table 2. The electrode surface area was controlled at 20 cm^2 with electrode length of 100 mm.
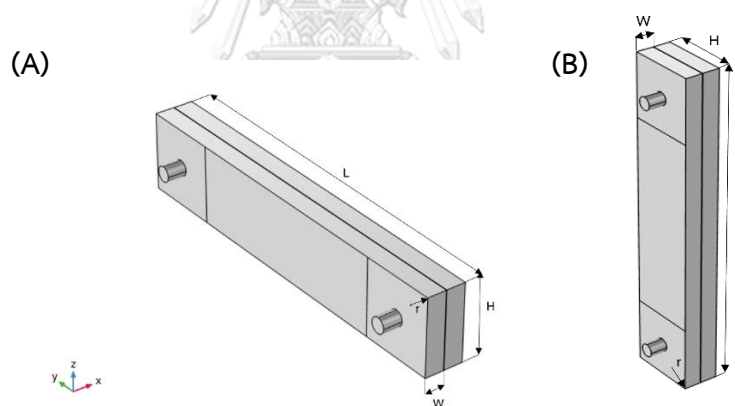
Figure 16. Schematic for a 3-D PEC reactor.

(A) horizontal and (B) vertical orientation.

Table 2. 3-D PEC reactor dimensions.

Parameter	unit	value
Reactor length (L)	mm	140
Channel width (W)	mm	5
Reactor heigh (H)	mm	20
Edge radius (r)	mm	0,5,10

Table 3. Modeling parameters.

Parameters			Value	Ref.
Equilibrium potential (V)		H_2	0.00	
		Benzaldehyde	0.26	[1]
Diffusion coefficient (m^2/s)		H^+	9.312×10^{-9}	[17]
		Benzyl alcohol	1.55×10^{-9}	
		Benzaldehyde	1.61×10^{-9}	
		H_2	5.11×10^{-9}	[17]
		Na_2SO_4	1.80×10^{-9}	[19]
Membrane diffusion coefficient (m^2/s)		H^+	1.33×10^{-9}	[20]
Membrane conductivity (S/m)			0.4	[21]
Exchange current densities (A/cm^2)		H_2	8.7×10^{-5}	[18]
		Benzaldehyde	2×10^{-13}	[18]
Transfer coefficients	anode	α_α	0.85	[18]
		α_c	0.1	[18]
	cathode	α_α	0.5	[18]
		α_c	0.5	[18]
Initial concentrations (mol/m^3)		Benzyl alcohol	0.2	[1]
		Benzaldehyde	1×10^{-4}	
		H^+	1×10^{-4}	
		OH^-	1×10^{-4}	
		Na^+	200	
		SO_4^{2-}	100	
		H_2	0.78	[18]
		Na_2SO_4	100	[1]
Electrode conductivity (S/m)		Pt	9.4×10^6	
		TiO_2 thin film on FTO glass	1×10^{-4}	[22]

3.2 Modeling equations

Photoelectrochemical reactor for benzyl alcohol oxidation paired with hydrogen production was simulated by using the following assumptions:

1. PEC reactor model was simulated as a single-phase model.
2. Laminar flow regime was used.
3. Incompressible fluid.
4. H_2 bubbles do not affect to the velocity profile in PEC reactor.

3.2.1 Light absorption

Solar radiation is the main driving force of many photochemical reactions that is affected by many factors including reflection and absorption from particles in the atmosphere. Therefore, a relatively more accurate estimation can be traced back from the standard reference solar spectra ASTM G173-03 at air mass (AM) 1.5[23] by calculating the incident photocurrent density using equation (24). [24]

$$i = q \int_{\lambda_1}^{\lambda_2} \frac{L\lambda}{hc} d\lambda \tag{24}$$

where i is an incident photocurrent density (A/m^2),

q is an elementary charge (1.6022×10^{-19}C),

h is Planck's constant (6.626×10^{-34} m^2·kg/s),

L is Spectral irradiance (W/m^2·nm),

c is light velocity (2.998×10^8 m/s).

3.2.2 Fluid flow

To study fluid behavior in the reactor, it was assumed to be a steady-state and an incompressible flow within z-direction. Therefore, the continuity equation is expressed by equation (25).

$$\frac{\partial(\rho v)}{\partial z} = 0 \tag{25}$$

where ρ is fluid density (kg/m^3),

v is fluid velocity in z direction (m/s).

The flow of electrolytes was assumed to be a laminar flow regime where Reynold numbers, Re < 2300. Therefore, the inlet velocity of fluid was calculated following equation (26).

$$v = \frac{\mu Re}{\rho D}$$ (26)

where μ is fluid dynamic viscosity (kg/m·s),

      ρ is fluid density (kg/m^3),

      D is the characteristic diameter (m),

      Re is Reynolds number.

To characterize the fluid momentum in z-direction, Navier-Stokes equations which describe momentum conservation, were used in equation (27).

$$v \frac{\partial(\rho v)}{\partial z} = -\frac{\partial P}{\partial z} + \mu\left(\frac{\partial^2 v}{\partial z^2}\right) + \rho g_z$$ (27)

where P is pressure (Pa),

      ρ is fluid density (kg/m^3),

      v is fluid velocity in z-direction (m/s),

      μ is fluid dynamic viscosity (kg/m·s),

      g_z is gravitational acceleration (9.81 m/s^2).

3.2.3 Charge transport

The charge transport by diffusion, migration, and convection in the liquid electrolyte were estimated using Nernst-Planck's equation. The chemical reaction, the molar flux, and electrolytic current of all species were respectively calculated using equations (28), (29), and (30)

$$R_i = \frac{\partial c_i}{\partial t} + \nabla \cdot \left(-D_i\nabla c_i - z_i u_{m,i} F c_i \nabla\phi_l\right) + u \cdot \nabla c_i \qquad (28)$$

$$N_i = -D_i\nabla c_i - z_i u_{m,i} F c_i \nabla\phi_l + u c_i \qquad (29)$$

$$i_l = F \sum_i z_i \left(-D_i\nabla c_i - z_i u_{m,i} F c_i \nabla\phi_l\right) \qquad (30)$$

where c_i is the concentration of specie i (mol/m³),

D_i is diffusion coefficient of specie i (m²/s),

z_i is charge number of specie i,

$u_{m,i}$ is the ionic mobility of specie i (m²/V·s),

F is Faraday's constant (96,485 C/mol),

ϕ_l is electrolyte potential (V).

3.2.4 Electrochemical kinetics

Butler Volmer's equation was used to estimated electrokinetics in the reactor model for both the anolyte and catholyte sides as shown in equation (31)

$$i = i_0 \left\{ exp\left(\frac{\alpha_a F\eta}{RT}\right) - exp\left(\frac{-\alpha_c F\eta}{RT}\right) \right\} \qquad (31)$$

where i_0 is exchange current densities,

α_a is anodic charge transfer coefficients,

α_c is cathodic charge transfer coefficients,

R is the gas constant (J/mol·K),

T is the reactor temperature (298 K),

η is the overpotential (V).

At the electrode/electrolyte interfaces, overpotential (η) was calculated from equation (32).

$$\eta = \phi_s - \phi_l - \phi_0 \qquad (32)$$

where ϕ_s is electric potential (V),

ϕ_l is electrolyte potential (V),

ϕ_0 is equilibrium potential (V).

CHAPTER 4

RESULTS AND DISCUSSION

Results from both analytical and numerical analyses are discussed in three sections. For the first section, benzyl alcohol oxidation and hydrogen reduction over electrode surface are discussed. The effects of electrolyte velocity and PEC reactor design are discussed in the second and the third sections, respectively.

4.1 Benzaldehyde and hydrogen concentrations

In this study, benzyl alcohol oxidation and hydrogen production were simulated in stationary with initialization study. The concentration distributions were observed with a minimum controlled velocity of 0.002 m/s which have the highest concentration gradient. The channel width and electrode length were controlled at 5 mm and 100 mm, respectively. Figure 17 shows the concentrations of hydrogen in catholyte channel and benzaldehyde in anolyte channel with 5 mm distance away from inlet and outlet of reactor. The concentration contours show that both of hydrogen and benzaldehyde concentration increased from the initial value at the surface of both electrodes. Hydrogen concentration on the cathode surface in catholyte channel is increased up to 4.5 mol/m^3 and the maximum benzaldehyde concentration on the photoanode surface is around 0.12 mol/m^3. According to figure 17, the obvious variation is observed only near the electrode surface where electrochemical reaction takes place. The concentration contour of hydrogen distributed more uniformly across the cathode surface than the concentration contour of benzaldehyde due to higher diffusivity of hydrogen.
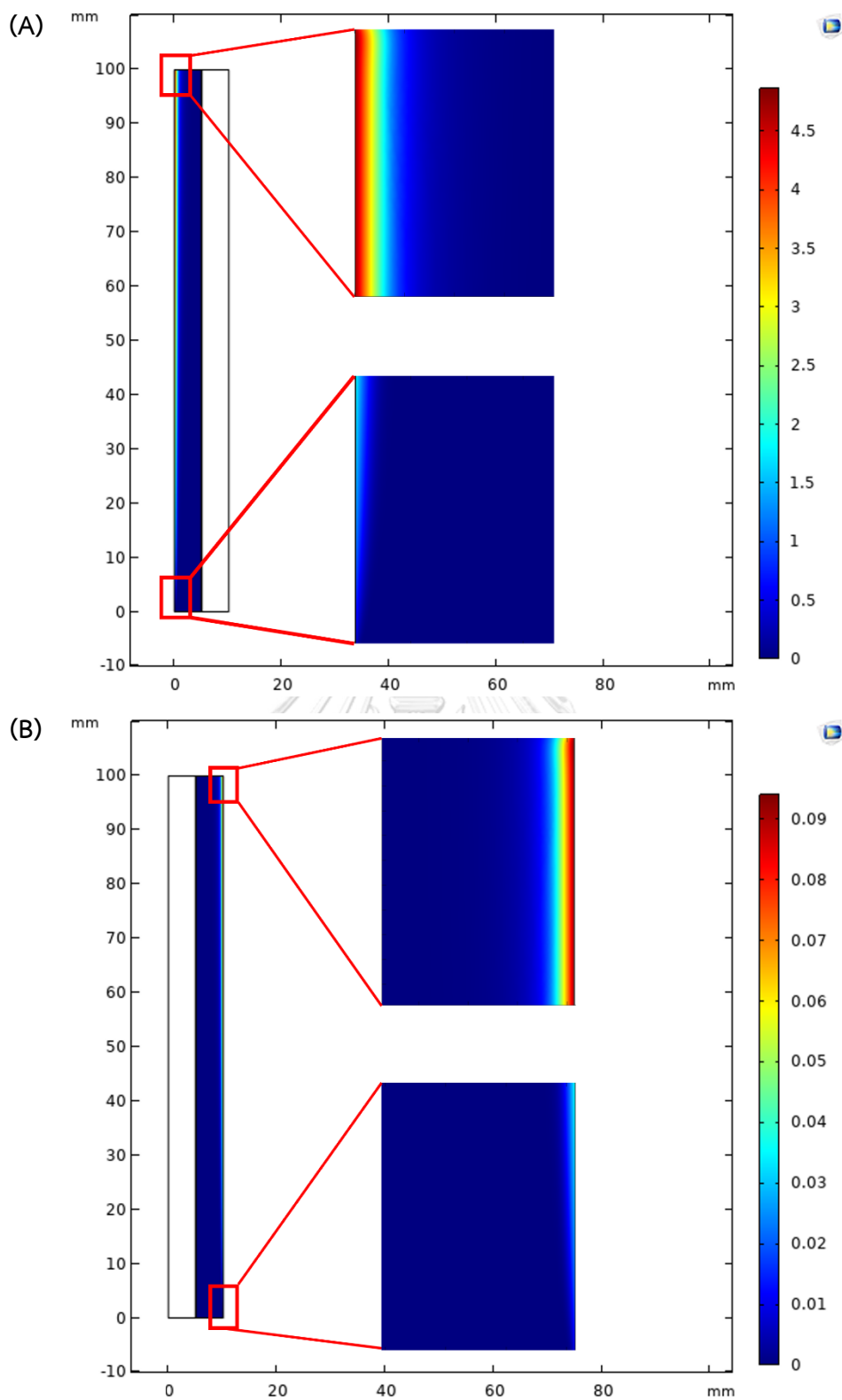
Figure 17. Concentrations of products at electrode surfaces. (A) hydrogen concentration at the cathode surface, and (B) benzaldehyde concentration at the photoanode surface.

(A)

(B)
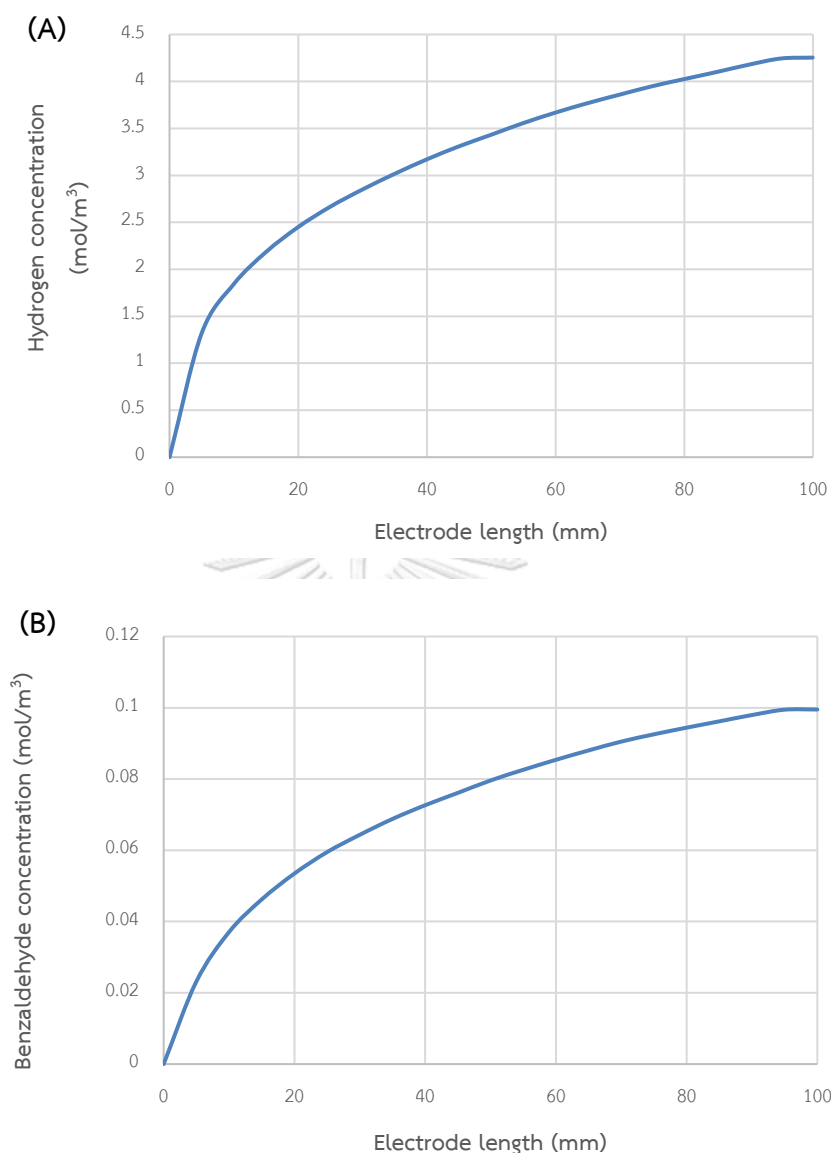
Figure 18. Concentration of products on electrode surface at 0.002 m/s with reactor length (A) hydrogen on cathode surface, and (B) benzaldehyde on anode surface.

The concentration of hydrogen and benzaldehyde at electrode surface are plotted along with electrode length of 100 mm as shown in figure 18. The concentration tends to be more intense towards the outlet of reactor.

Moreover, the concentrations of hydrogen and benzaldehyde at 100 mm electrode length were plotted with channel width as shown in figure 25 and 26 appendix C, respectively. Both hydrogen and benzaldehyde are formed only near the

electrode surface, while further away from the electrode surface, the concentration was decreased until it reached the initial value. It can be concluded that the diffusion step is not rate determining step.

In addition, to ensure that the electrochemical reaction takes place at the electrode surface. The electrode current densities with the electrolyte current density vectors in catholyte and anolyte channels are shown in appendix C, figure 27 and 28, respectively. In addition, the electrolyte current density on the electrode surface in catholyte and anolyte are plotted with electrode length as shown in appendix C, figure 29 and 30, respectively. The current density vectors shown that the current flow from anolyte to catholyte channel. The anode current density is reduced due to the decrease in benzyl alcohol concentration along the anode length. However, the current density of cathode is increased along the cathode length because the concentration of proton is increased due to the transportation of proton from anolyte to catholyte channel.

4.2 Effects of electrolyte flow velocity

As mentioned in previous section, product accumulation is unavoidable in a practical PEC reactor. Therefore, the influence of electrolyte flow velocity was investigated. The study of stationary and time dependent with initialization were used in this simulation.

1. Stationary with initialization study

The relationship between hydrogen and benzaldehyde concentrations and electrode length is shown in figure 19(A) and (B), respectively. Electrolyte flow velocity was varied at 0.002, 0.004, and 0.006 m/s to obtain the laminar flow regime. Hydrogen and benzaldehyde concentrations were observed at above 0.1 mm from the electrode surface with 100 mm length of reactor. From figure 19(A), hydrogen concentration decreased with increasing electrolyte velocity from 0.002 to 0.006 m/s. At 100 mm electrode length, hydrogen concentration at 0.006 m/s has the lowest

concentration of about 2.6 mol/m^3 while the velocity at 0.002 m/s results in the highest concentration of 4.3 mol/m^3. In figure 19(B), benzaldehyde concentration on the photoanode surface of 100 mm length with velocity 0.006 m/s is 0.05 mol/m^3, while the concentration obtained from electrolyte velocity of 0.002 m/s is 0.1 mol/m^3. From the simulation results, benzaldehyde concentration at the photoanode surface also decreased with the same trend of hydrogen concentration at the cathode surface.
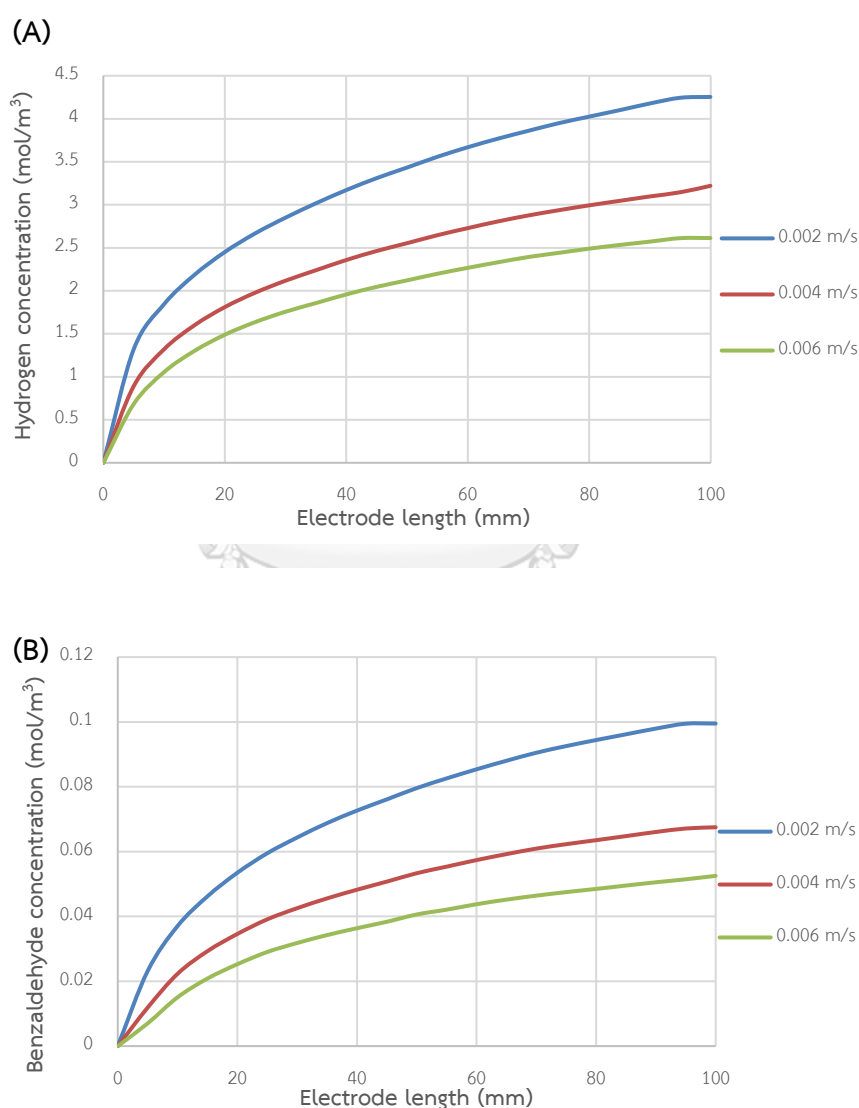

Figure 19. Effects of electrolyte velocity on concentrations of (A) hydrogen, and (B) benzaldehyde at 0.002 m/s, 0.004 m/s and 0.006 m/s.

Figure 19(A) and (B) clearly show that the concentrations of hydrogen and benzaldehyde decrease with increasing electrolyte flow velocity due to shear force from electrolyte flow velocity. This indicates that product accumulation which was formed at the electrode surface can be removed by increasing the electrolyte flow velocity. Sivula and Grätzel [25] have referred to the fact that electrolyte flow adds an extra force to shear the product accumulation from the electrode surface. According to this statement, the lower velocity, the lesser the shearing force and the more the product accumulation. Therefore, higher velocities reduce the gas or products off the electrode surface.

2. Time dependent with initialization study

This section was simulated to study the lifetime of PEC reactor due to the product accumulation. Electrolyte flow velocity was controlled at 0.002 m/s. The concentration of hydrogen and benzaldehyde were plotted with electrode length with varied time 0 to 600 second as shown in figure 41 and 42 in appendix D. From figure 41, hydrogen concentration was increased with time on cathode surface. After 180 second, hydrogen concentration remains the same. In figure 42, benzaldehyde concentration was increased with time on photoanode surface. There is no change in benzaldehyde concentration when reaction time more than 300 second.

From results of time dependent study, it can be concluded that, lifetime of PEC reactor for benzyl alcohol oxidation is about 300 second. In addition, if more product is accumulated on the electrode surface, it may cause an increase in electrical resistant due to the thickness of product accumulation on the electrode surface. Thus, the higher velocity of electrolyte should be used to reduce the product accumulation on electrode surface due to the higher shear force.

4.3 PEC reactor design

In this section, the effects of electrolyte channel width are discussed to determine the optimal channel width for a 3D PEC reactor of benzyl alcohol oxidation simulation.

4.3.1 Effects of electrolyte channel width

To investigate effects of electrolyte channel width, electrolyte flow velocity was maintained at 0.002 m/s in laminar flow regime. Length of electrode was controlled at 100 mm as a practical PEC reactor. Both of catholyte and anolyte channel width were varied from 5 to 50 mm with intervals of 10 mm. PEC reactor simulation was carried out through stationary with initialization and time dependent with initialization.

1. Stationary study

This study was simulated in stationary with initialization to investigate the effects of electrolyte channel width. The relationship of hydrogen and benzaldehyde concentration at electrode surface over the reactor length with varied electrolyte channel width are shown in figure 20. From figure 20(A), at the outlet of the reactor, the hydrogen concentration obtained from the catholyte channel width of 5 mm is 4.79 mol/m^3, and increased to 5.38, and 5.60 mol/m^3 with wider channel widths of 10 and 20 mm, respectively. After that, hydrogen concentration is decreased to 5.38, 5.00, and 4.79 mol/m^3 with further wider channel widths of 30, 40, and 50 mm, respectively. The effects of the anolyte channel width on benzaldehyde concentration at the outlet of reactor are shown in figure 20(B). The average benzaldehyde concentration obtained at the outlet of the reactor with anolyte channel width 5 mm is 0.09 mol/m^3 and increased to 0.15 mol/m^3 with wider anolyte channel of 20 mm. After that, benzaldehyde concentration is slightly increased to 0.17 mol/m^3 with channel width of 50 mm. However, it can be observed that when the channel is wider from 20 to 50 mm, gaps of each curve are getting closer to each other.
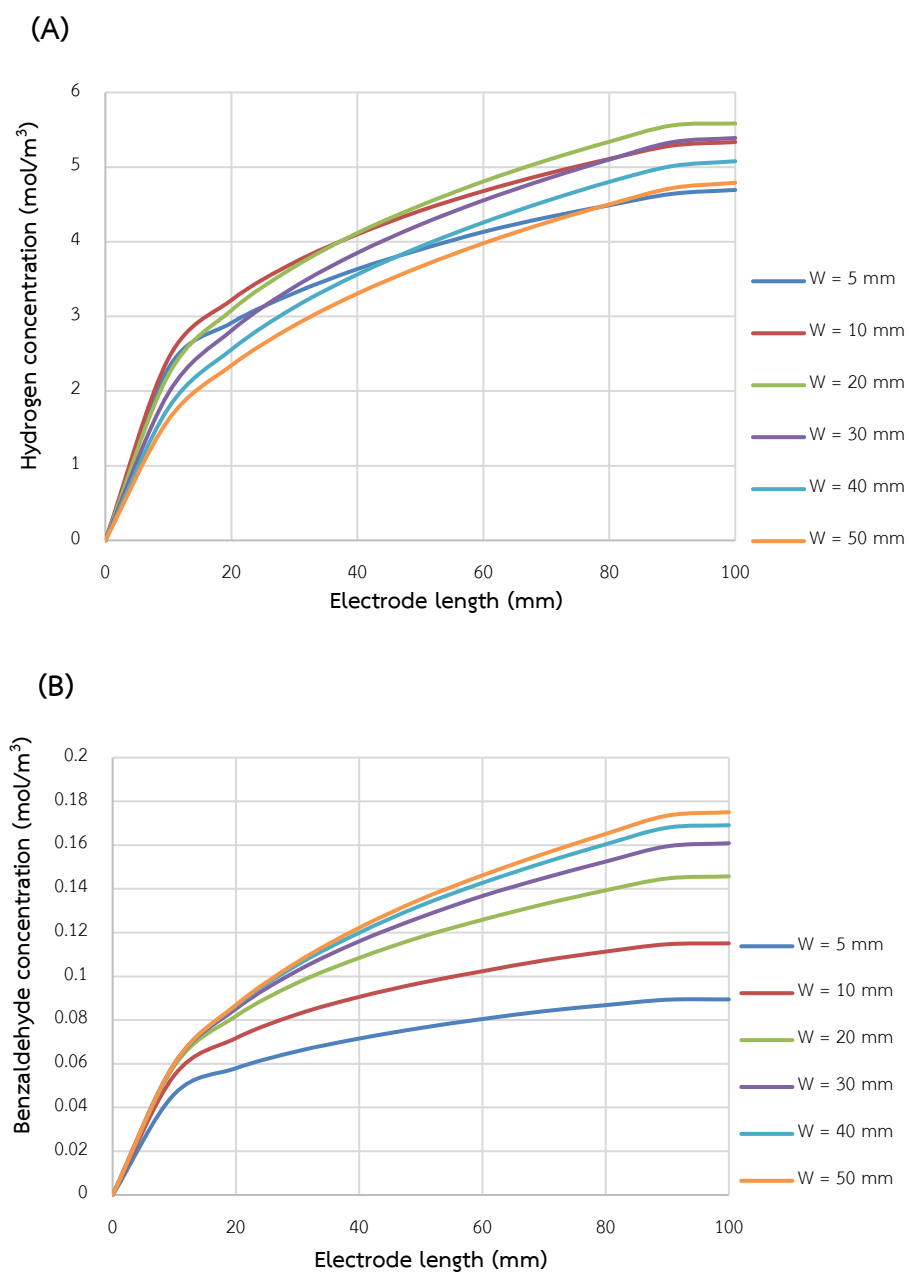
(A)

(B)

Figure 20. Concentrations of products at electrode surface of electrode length of 100 mm with varied channel widths. (A) hydrogen concentration with varied catholyte channel width from 5 to 50 mm and (B) benzaldehyde concentration with varied catholyte channel width from 5 to 50 mm.

From these results, it is clear that when the electrolyte channel is wider, this allows more volumes of electrolyte and reactant to flow into the channel of PEC reactor. However, when the channel is wider than 20 mm, the concentration of hydrogen in catholyte channel at the cathode surface was significantly decreased and benzaldehyde concentration in anolyte channel is slightly increased. According to the simulation results, if the channel width is increased, it may affect the potential distribution within the reactor. Thus, the relation between channel width with electrolyte potential is shown in figure 21.
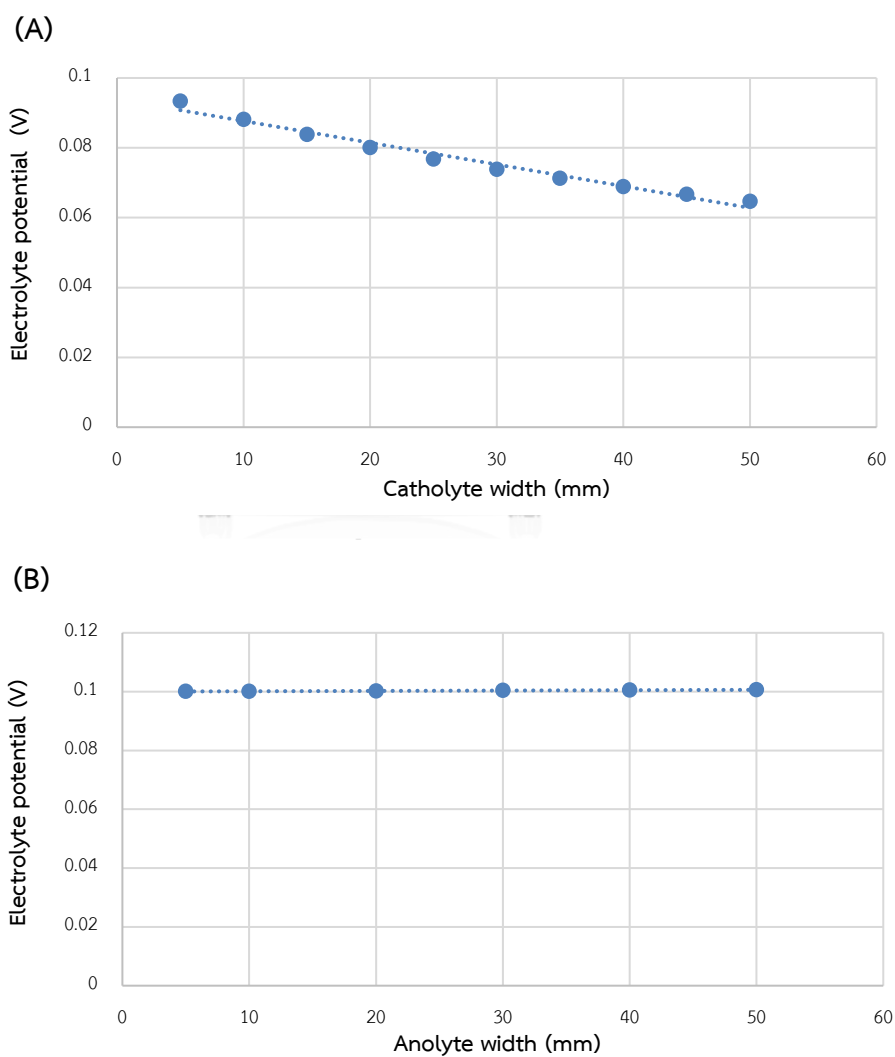
(A)

(B)

Figure 21. Electrolyte potentials at electrode surface with varied channel widths (A) catholyte channel and (B) anolyte channel.

Figure 21 shows the electrolyte potential or cell potential across the channel with varied width. The determined electrolyte potentials and corresponding trendline at the cathode surface in catholyte channel with varied catholyte channel width is shown in figure 21 (A). Electrolyte potential calculated from the 5 mm catholyte channel width is 0.09 V, and decreased to 0.06 V with 50 mm catholyte channel width. Figure 21 (B) shows the determined electrolyte potentials and corresponding trendline at the photoanode surface with varied anolyte channel width. It can be seen that anolyte channel width do not affect to the electrolyte potential on the photoanode surface.

In cathode, electrolyte potential drops with wider catholyte channel while electrolyte potential is not changed on the photoanode surface. Therefore, it can be concluded that when the channel is too wide, this can cause Ohmic potential drop and poor potential distribution , especially in the catholyte. The electrolyte potential in the PEC reactor flows with protons through the proton exchange membrane from the anode to the cathode. Charge transport of hydrogen is calculated in terms of diffusion and migration by using Nernst-Planck's equation as shown in equation 29. There are many factors that can affect the rate of diffusion and migration. including temperature, concentration difference, and distance, etc. The distance between the electrodes is important factor that can affect both diffusion rate and electrochemical rate. Thus, the shorter distance that substance has to move, the rate of diffusion becomes faster. If the channel is too wide, the distance between photoanode and cathode is too large. The potential distribution problem in PEC reactor can be occurred and affect the rate of electrochemical at electrode surface because one of the factors that can affect the electrochemical rate is electrolyte potential. The electrochemical reactions are described as a function of the overpotential (η). The general expression of Butler-Volmer and overpotential are shown in equations 31, and 32, respectively.

$$N_i = -D_i\nabla c_i - z_i u_{m,i} F c_i \nabla \phi_l + u c_i \tag{29}$$

$$i = i_0 \left\{ exp\left(\frac{\alpha_a F \eta}{RT}\right) - exp\left(\frac{-\alpha_c F \eta}{RT}\right) \right\} \tag{31}$$

$$\eta = \phi_s - \phi_l - \phi_0 \tag{32}$$

It is clear that overpotential directly affects the charge transfer current density (i), which affects the rate of electrochemical of the electrode surface in the transport of diluted species interface as expressed in equation (33).

$$R = \frac{\nu_i i}{nF} \tag{33}$$

2. Time dependent study

The effects of electrolyte channel width were also simulated in time dependent with initialization to investigate hydrogen and benzaldehyde concentration over time 0 to 300 seconds with time interval of 60 seconds. Hydrogen and benzaldehyde concentrations on electrode surfaces at 100 mm electrode length were observed over time with varied channel widths from 5 to 50 mm, as shown in figure 22(A) and (B).

At the outlet of catholyte channel in figure 22(A), hydrogen concentration of all channel widths has the same trend where it is increased with time. At 5 to 10 mm channel width, hydrogen concentration increases. When the channel is wider than 10 mm, the trend of hydrogen concentration at the outlet of reactor over time significantly decreases, which is similar to the stationary with initialization study section. In figure 22(B), benzaldehyde concentration of all channel widths also has the same trend where it is increased with time. Moreover, concentration of benzaldehyde increases with wider anolyte channel, but when anolyte channel is greater than 10 mm, the trend line of each channel width becomes very closer to each other.
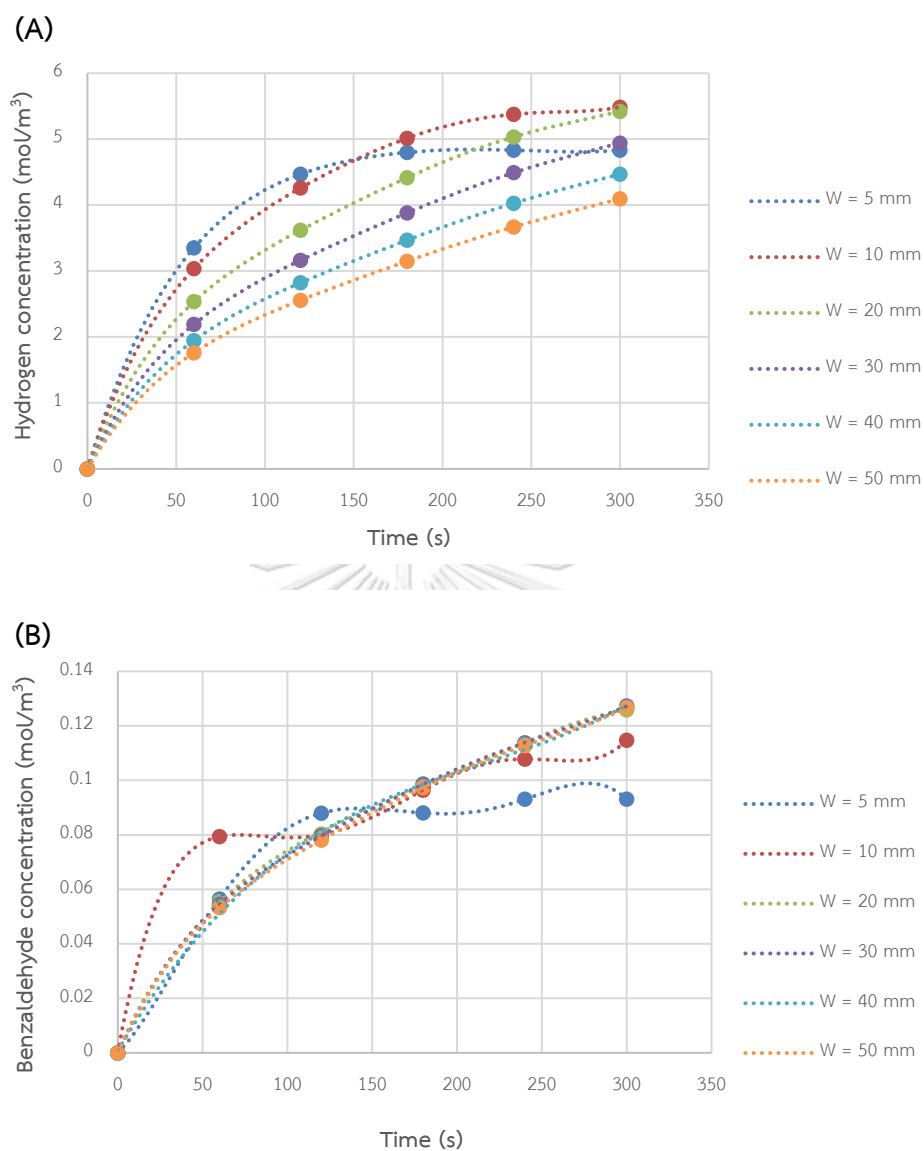
(A)

(B)

Figure 22. Concentrations of products on electrode surfaces at electrode length of 100 mm with time and varied channel widths. (A) Hydrogen concentration with varied anolyte width and (B) Benzaldehyde concentration with varied catholyte width.

At the outlet of catholyte channel in figure 22(A), hydrogen concentration of all channel widths has the same trend where it is increased with time. At 5 to 10 mm channel width, hydrogen concentration increases. When the channel is wider than 10 mm, the trend of hydrogen concentration at the outlet of reactor over time significantly decreases, which is similar to the stationary with initialization study section. In figure 22(B), benzaldehyde concentration of all channel widths also has the same trend where it is increased with time. Moreover, concentration of benzaldehyde increases with wider anolyte channel, but when anolyte channel is greater than 10 mm, the trend line of each channel width becomes very closer to each other.

From all results of both stationary study and time dependent study, it indicates that the distance between two electrodes directly affects the concentration of the products. If the distance between two electrodes is too large, it can cause problems in terms of potential distribution from the photoanode to the cathode. However, if the distance between two electrodes is too small, resulting in a smaller reactor volume, lesser volume of electrolyte and reactant can flow into the reactor. Thus, it is important to keep the optimal distance between the electrodes to obtain the maximum efficiency PEC reactor.

4.3.2 3-dimensional (3-D) PEC reactor

Table 4. Configuration of 3-D PEC reactor in horizontal and vertical orientation.
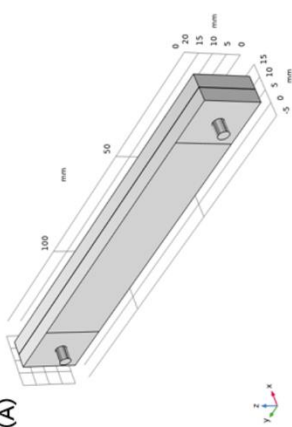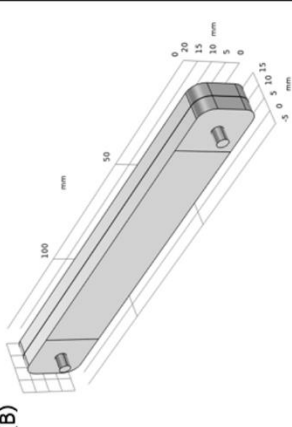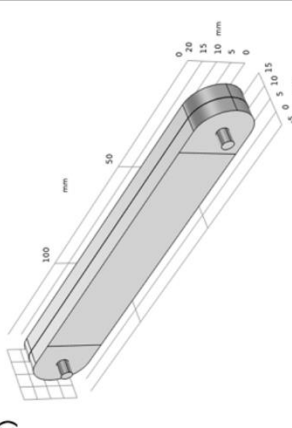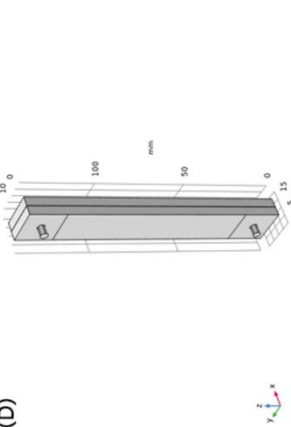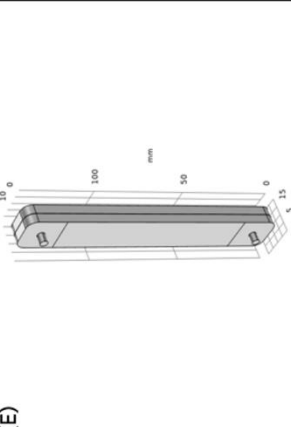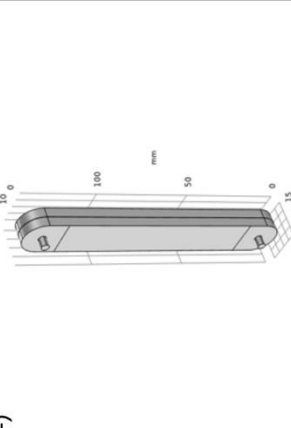
Table 5. Velocity contours with velocity field for 3-D PEC reactor model simulation in horizontal and vertical orientation.
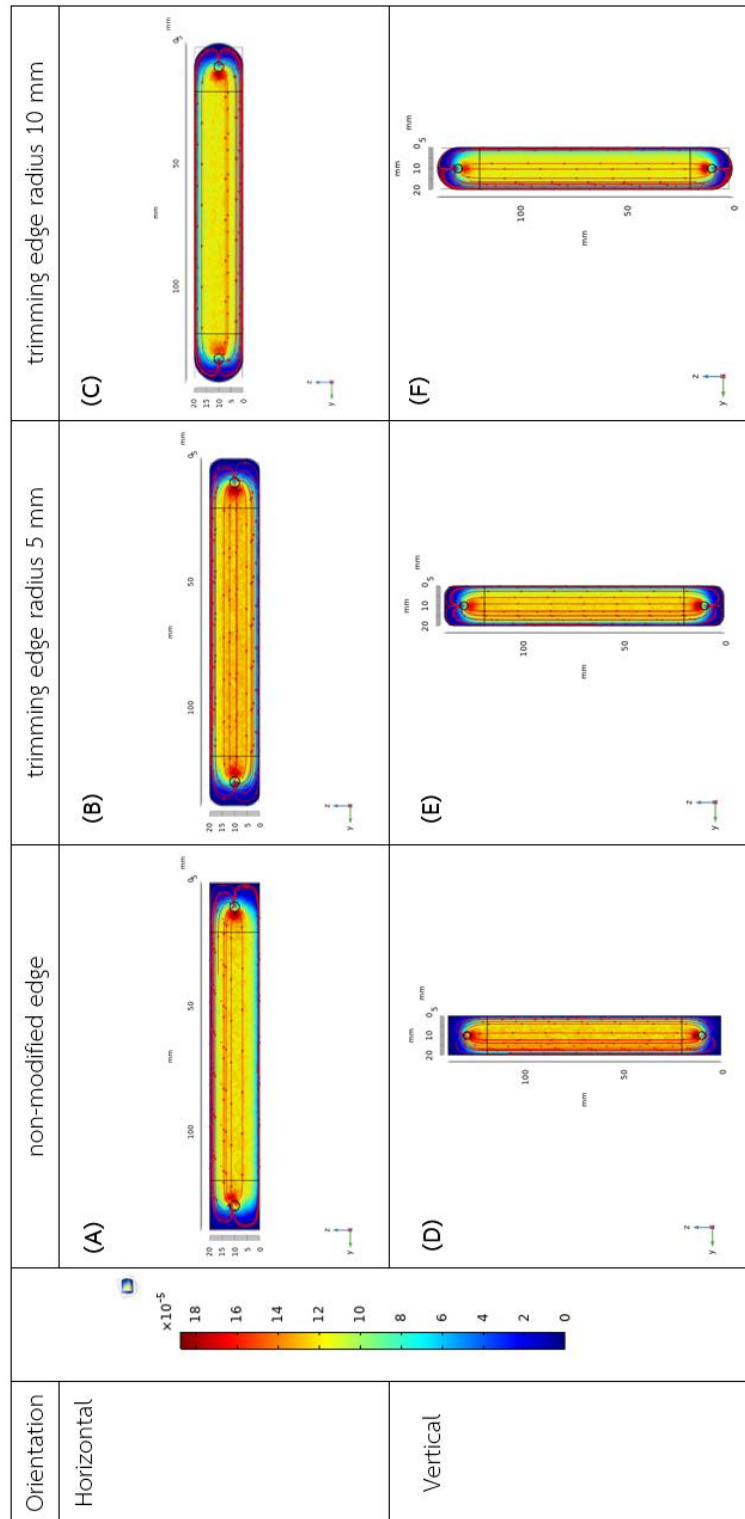
To simulate and determine the optimal configuration and orientation of 3D PEC reactor, electrolyte flow velocity was maintained at 0.002 m/s due to the highest concentration gradient on electrode surface. Electrode surface area was controlled at 12 cm^2 and placed in the middle of reactor wall. As mentioned in section 4.3.1, channel width was controlled at 5 mm with electrode length of 100 mm. This study was stationary with initialization study. The configuration and orientation of PEC reactor model investigated in this study is shown in table 4. The orientation of PEC reactor model consists of vertical and horizontal orientation. The configuration of PEC reactor model was modified by trimming edge radius of PEC reactor into 5 and 10 mm.

Velocity profile with streamline in 3D PEC reactor models are shown in table 5. All results show a velocity flow reflecting uniform linear motion which is characterization of a laminar flow, where streamlines cannot overlap to each other. Velocity contour with streamline of non-modified reactor model is shown in figure A, horizontal orientation and figure D, vertical orientation within table 5. This model has the most area of low velocity zone or dead zone (dark blue zone) for both vertical and horizontal orientation. Figure B and E show the velocity contour with streamline of 5 mm trimmed edge radius of PEC reactor. In this model, the dark blue zone is lesser than that of the non-modified model. The last modified PEC reactor model is 10 mm trimmed edge radius of PEC reactor model, as shown in figure C and F. This modified PEC reactor model has the lowest low velocity zone. Moreover, the average concentrations of hydrogen, benzaldehyde, and benzyl alcohol at the outlet are shown in table 7 to 9 in appendix C, respectively. The concentrations of all species in each PEC reactor model are not significantly different because surface area of electrode that electrochemical reaction take place was controlled at the same value.

In addition, pressure drop of all PEC reactor models is shown in table 10 in appendix C. According to the assumption that is hydrogen bubbles do not affect to the velocity profile in PEC reactor. Thus, only hydro static pressure affected the

pressure drop in PEC reactor. The pressure between inlet and outlet point in PEC reactor model with horizontal orientation was not significantly different because the inlet and outlet of the reactor are at a height of 10 mm in the z-axis as shown in figure 24(A) appendix C. Thus, there is slightly pressure drop around 0.5 - 0.7 Pa in horizontal PEC reactor model. However, pressure drop in vertical PEC reactor model is very high because the inlet and outlet of the reactor are at different heights as shown in figure 24(B) in appendix C. The pressure at the inlet of PEC reactor model was measured at a height of 10 mm while the pressure at outlet of the reactor was measured at 90 mm, thus the pressure drop in the vertical PEC reactor model is higher than the pressure drop in the horizontal PEC reactor model.

According to the results, the modified radius edge of PEC reactor model can improve the velocity flow profile and can decrease the low velocity zone in PEC reactor. However, the concentration of hydrogen and benzaldehyde are not affected because the electrode surface area that electrochemical reaction takes place was controlled at the same value in all PEC reactor models. Moreover, the vertical PEC reactor has higher pressure drop than that of the horizontal PEC reactor. When a higher pressure drop occurs in the PEC reactor, the higher pumping power is required. Therefore, to reduce the effects of pressure drop, the horizontal PEC reactor is the best choice to construct the real PEC reactor for benzyl alcohol oxidation coupled with hydrogen production.

CHAPTER 5

CONCLUSIONS

5.1 Conclusions

In this present work, charge transport and fluid flow phenomena including electrochemical kinetics of a 2-D of PEC reactor model was numerically investigated. The configuration and orientation of 3-D PEC reactor model were studied. Both stationary and time dependent study were used in this research. The proton exchange membrane was also included in the simulations for product separation in PEC reactor model. It can be concluded as follows:

1. The concentration contour of hydrogen distributed more uniformly across the cathode surface than the concentration contour of benzaldehyde on the photoanode surface due to its higher diffusivity and tends to be more intense towards the outlet of reactor.

2. The product accumulation which was formed at the electrode surface can be reduced by increasing the electrolyte flow velocity due to the higher shear force.

3. The distance between two electrodes directly affects the concentration of the products. If the distance between two electrodes is too large, it can cause problems in terms of potential distribution from the photoanode to the cathode. However, if the distance between two electrodes is too small, resulting in a smaller reactor volume, lesser volume of electrolyte and reactant can flow into the reactor.

4. The modified radius edge of PEC reactor model can improve the velocity flow profile and can decrease the low velocity zone in PEC reactor. However, the concentration of hydrogen and benzaldehyde are not affected because the electrode surface area that electrochemical reaction takes place was controlled at the same value in all PEC reactor model.

5. The PEC reactor model with vertical orientation has higher pressure drop than horizontal orientation. When a higher pressure drop occurs in the PEC reactor, the higher pumping power is needed. Therefore, to reduce the effects of

pressure drop, the horizontal PEC reactor is the best choice to construct the real PEC reactor for benzyl alcohol oxidation coupled with hydrogen production.

5.2 Recommendations for the future work

1. Investigate the effect of the distance of light source to estimate the optimal distance between photoanode and light source.

2. Investigate and simulate another type of PEC reactor model, such as a front-illuminated model, to determine the best PEC reactor type for benzyl alcohol oxidation reaction.

จุฬาลงกรณ์มหาวิทยาลัย

CHULALONGKORN UNIVERSITY

APPENDIXES

Appendix A: Diffusivity calculation

The equation developed by Wike and Chang (1955) can be used to predict liquid diffusivity:

$$D_L = \frac{1.173 \times 10^{-13}(\phi M)^{0.5}T}{\mu V_m^{0.6}}$$

(35)

Where

D_L = liquid diffusivity, m^2/s;

ϕ = an association factor for the solvent;

M = molecular mass of solvent;

μ = viscosity of solvent, mPa·s;

T = temperature, K;

V_m = molar volume of the solute at its boiling point, m^3/kmol. This can be estimated from the group contributions given in figure 23.

Molecular Volumes

Air	0.0299	CO_2	0.0340	H_2S	0.0329	NO	0.0236
Br_2	0.0532	COS	0.0515	I_2	0.0715	N_2O	0.0364
Cl_2	0.0484	H_2	0.0143	N_2	0.0312	O_2	0.0256
CO	0.0307	H_2O	0.0189	NH_3	0.0258	SO_2	0.0448

Atomic Volumes

As	0.0305	F	0.0087	P	0.0270	Sn	0.0423
Bi	0.0480	Ge	0.0345	Pb	0.0480	Ti	0.0357
Br	0.0270	H	0.0037	S	0.0256	V	0.0320
C	0.0148	Hg	0.0190	Sb	0.0342	Zn	0.0204
Cr	0.0274	I	0.037	Si	0.0320		

Cl, terminal, as in RCl	0.0216	in higher esters, ethers	0.0110
medial, as in R—CHCl—R	0.0246	in acids	0.0120
Nitrogen, double-bonded	0.0156	in union with S, P, N	0.0083
triply bonded, as in nitriles	0.0162	three-membered ring	− 0.0060
in primary amines, RNH_2	0.0105	four-membered ring	− 0.0085
in secondary amines, R_2NH	0.012	five-membered ring	− 0.0115
in tertiary amines, R_3N	0.0108	six-membered ring as in	− 0.0150
		benzene, cyclohexane, pyridine	
Oxygen, except as noted below	0.0074		
in methyl esters	0.0091	Naphthalene ring	− 0.0300
in methyl ethers	0.0099	Anthracene ring	− 0.0475

Figure 23. Structural contributions to molar volumes, m^3/kmol (Gambill, 1958)

Table 6. Parameters for diffusivity of benzaldehyde and benzyl alcohol calculation.

Parameters	unit	Benzaldehyde	Benzyl alcohol	Ref.
ϕ		1		[26]
MW of Na_2SO_4	g/mol	142.04		
μ of Na_2SO_4 (at 298.15 K)	mPa·s	0.933		[27]
T	K	298.15		
V_m	m^3/kmol	0.1182	0.1256	

Find diffusivity of benzyl alcohol and benzaldehyde in Na_2SO_4:

$$D_{benzyl\ alcohol} = \frac{1.173 \times 10^{-13} (1 \times 142.04)^{0.5} (298.15)}{0.933 \times 0.1256^{0.6}}$$

$$= 1.5510 \times 10^{-9} \ m^2/s$$

$$D_{benzaldehyde} = \frac{1.173 \times 10^{-13} (1 \times 142.04)^{0.5} (298.15)}{0.933 \times 0.1182^{0.6}}$$

$$= 1.6087 \times 10^{-9} \ m^2/s$$

Appendix B: Electrolyte flow velocity calculation

Velocity can be determined from Reynold's number (Re) as follow equation 36.

$$Re = \frac{vL}{\nu} = \frac{\rho vL}{\mu}$$

(36)

Where
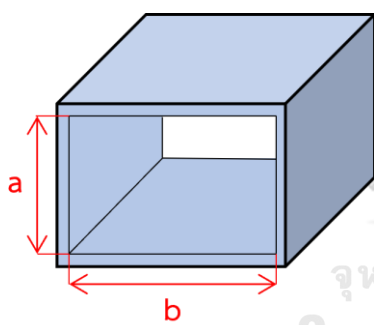
ρ is the density of the fluid, kg/m3;

v is the flow velocity, m/s;

L is a characteristic length, m;

μ is the dynamic viscosity of the fluid, Pa·s or N·s/m^2 or kg/(m·s)

For rectangular duct, the characteristic dimension is replaced to be the hydraulic diameter, D_h, defined as

$$D_h = \frac{4ab}{2(a+b)} = \frac{2ab}{a+b}$$

(37)

Find D_h:

$$D_h = \frac{2(5 \text{ mm})(20 \text{ mm})}{(5 \text{ mm}+20 \text{ mm})}$$

$$= 8 \text{ mm} = 0.008 \text{ m}$$

Find velocity at Re = 20:

$$Re = \frac{\rho vL}{\mu}$$

$$20 = \frac{(997 \frac{\text{kg}}{\text{m}^3})v(0.008 \text{ m})}{8.9 \times 10^{-4} \text{ kg/m·s}}$$

$$v = 0.002 \text{ m/s}$$

Appendix C: Simulation results for stationary study

Table 7. Average hydrogen concentration at outlet of reactor.

edge radius (mm)	average hydrogen concentration (mol/m^3)	
	Vertical	Horizontal
0	0.9679	0.9517
5	1.0049	1.1349
10	1.0013	1.1338

Table 8. Average benzaldehyde concentration at outlet of reactor.

edge radius (mm)	average benzaldehyde concentration (mol/m^3)	
	Vertical	Horizontal
0	0.1035	0.0965
5	0.1105	0.1136
10	0.1104	0.1136

Table 9. Average benzyl alcohol concentration at outlet of reactor and conversion percentage.

edge radius (mm)	average benzyl alcohol concentration (mol/m^3)		%Conversion	
	Vertical	Horizontal	Vertical	Horizontal
0	0.1035	0.1035	48.25	48.25
5	0.0897	0.0863	55.15	56.85
10	0.0894	0.0863	55.30	56.85

Table 10. Pressure drop in PEC reactor.

edge radius (mm)	Pressure (Pa)					
	Vertical			Horizontal		
	P_1	P_2	ΔP	P_1	P_2	ΔP
0	1,651	33.69	1,618	42.00	41.48	0.5240
5	1,665	47.07	1,618	46.71	46.00	0.7130
10	1,659	40.62	1,618	46.63	45.96	0.6780
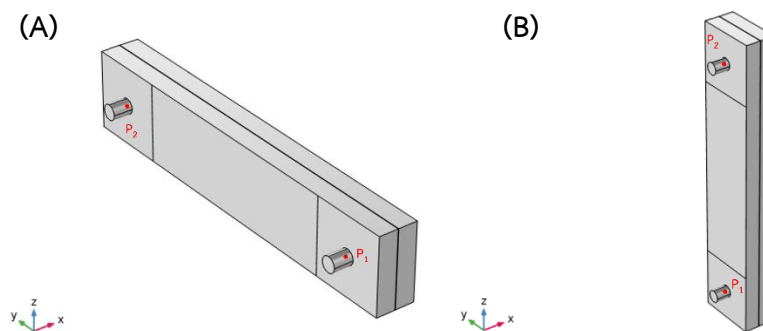
Figure 24. Inlet and outlet point for pressure drop calculation in PEC reactor model
(A) Horizontal orientation, and (B) Vertical orientation.
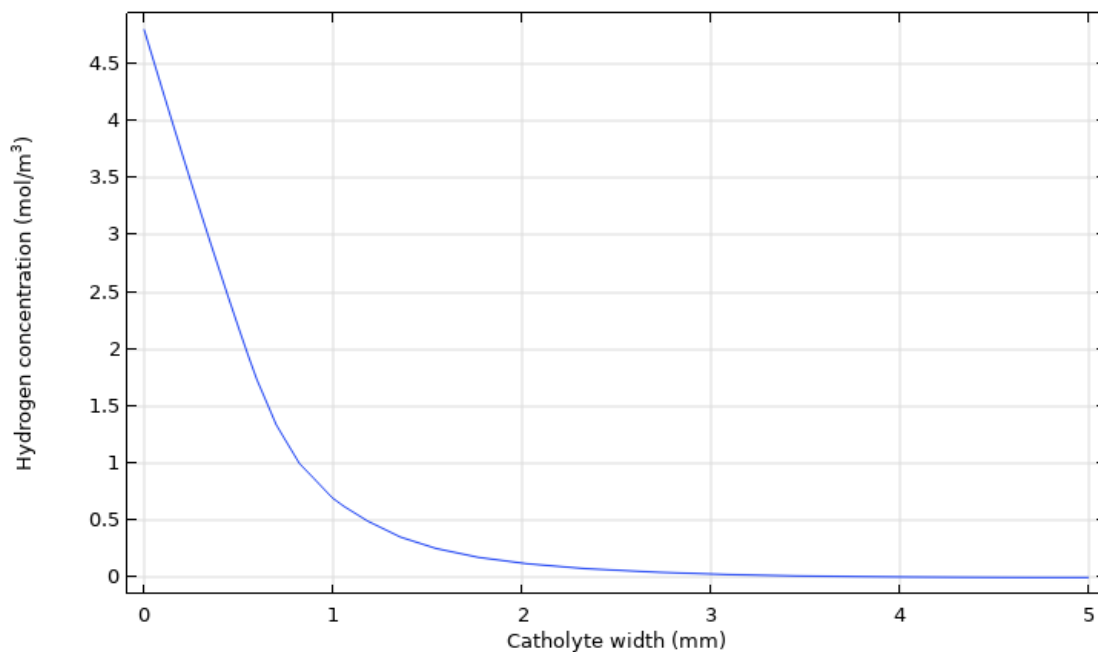
Figure 25. Hydrogen concentration across the catholyte width at 100 mm electrode length.
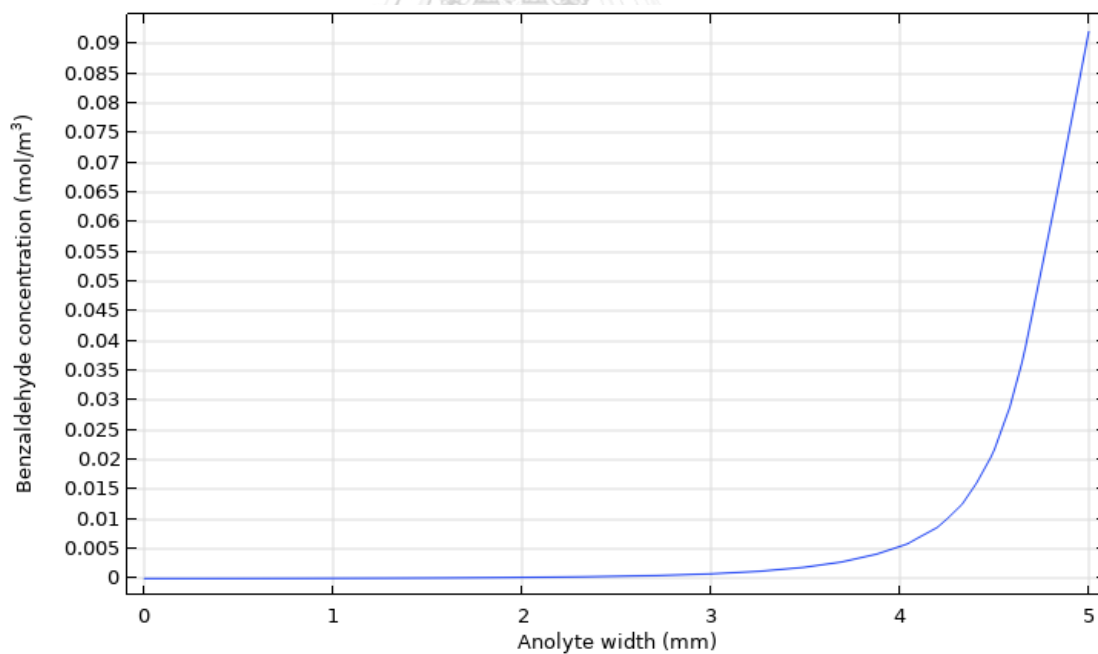
Figure 26. Benzaldehyde concentration across the anolyte width at 100 mm electrode length.
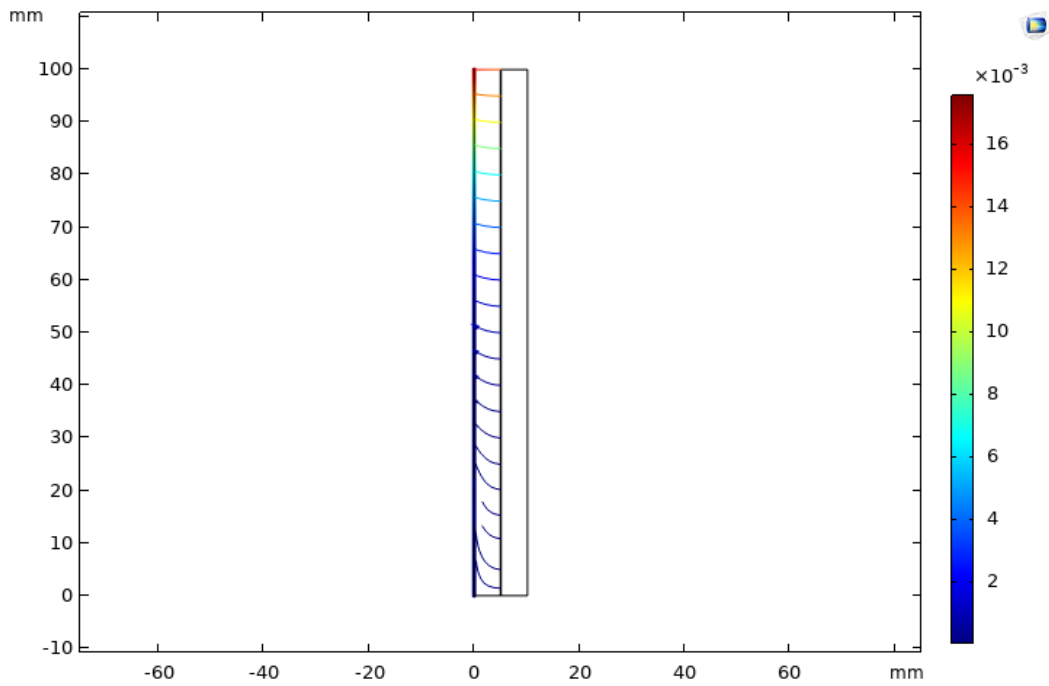
Figure 27. Electrode current density with electrolyte density vector in catholyte channel.
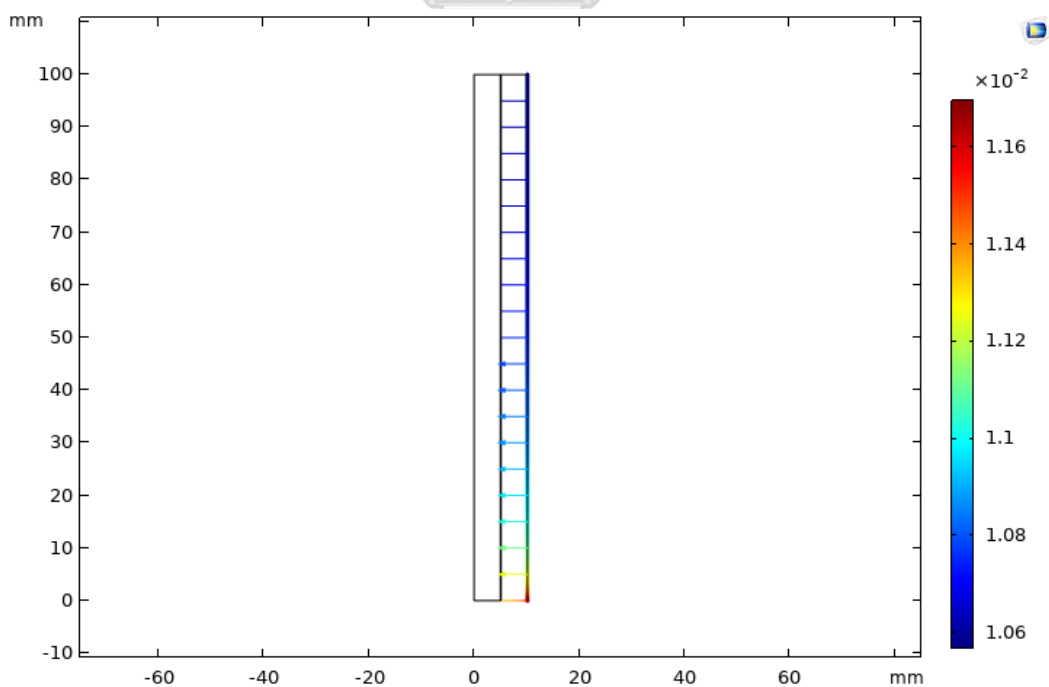
Figure 28. Electrode current density with electrolyte density vector in anolyte channel.
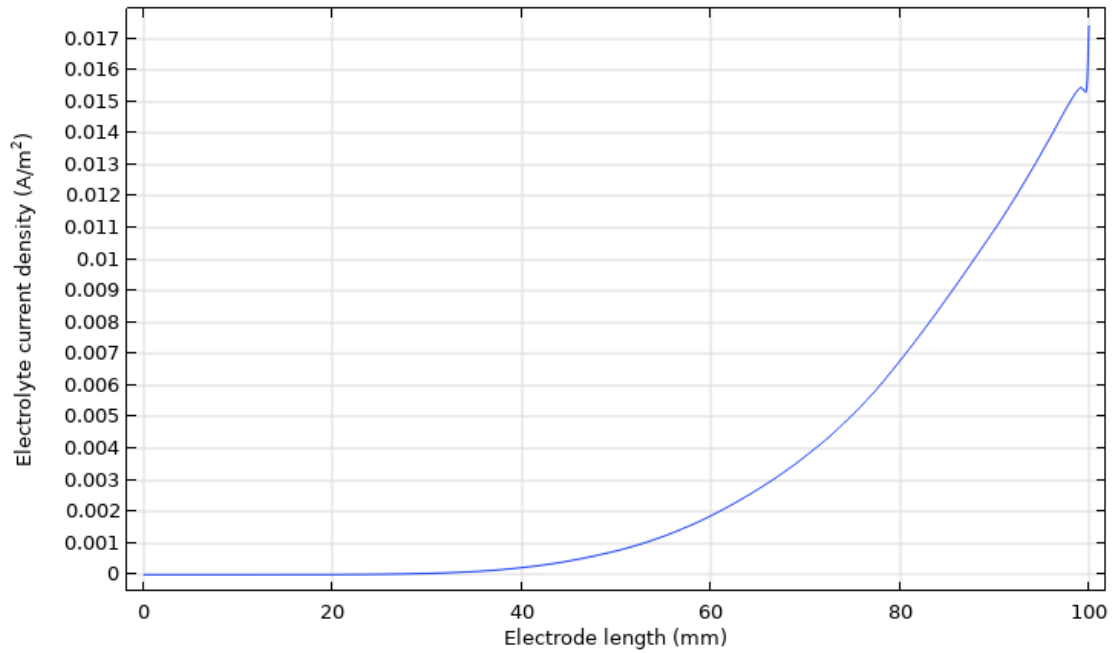
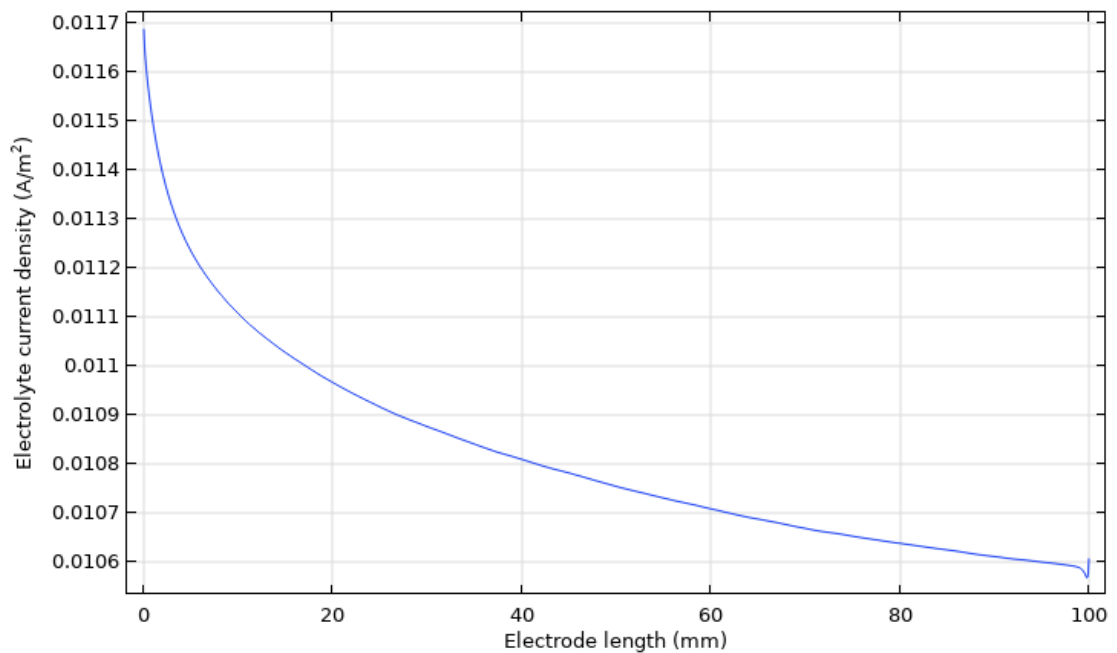**Figure 29.** Electrolyte current density with electrode length in catholyte channel.

Figure 30. Electrolyte current density with electrode length in anolyte channel.

Appendix D: Simulation results for time dependent study

1. Hydrogen concentration
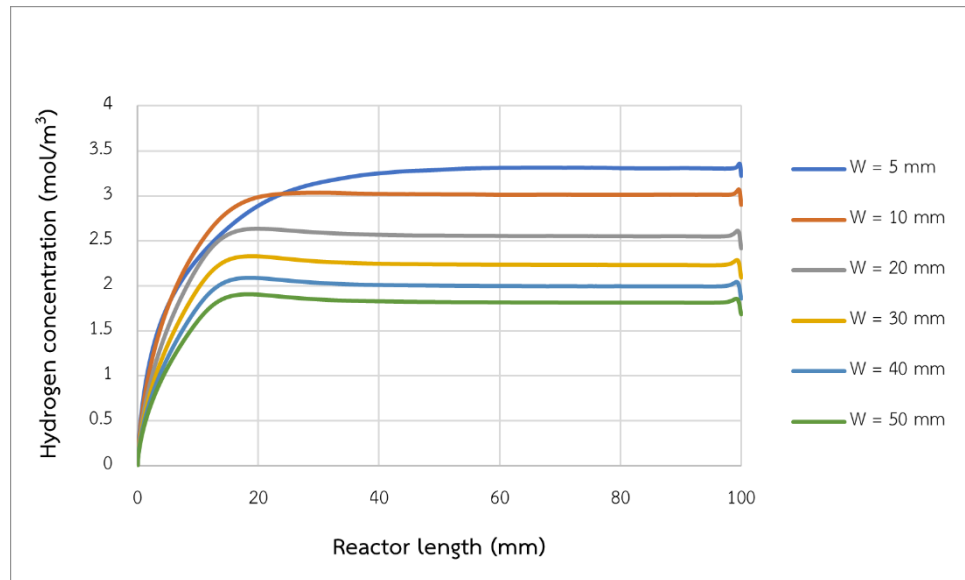
Figure 31. Hydrogen concentration over reactor length at time = 60 second with varied catholyte channel width.
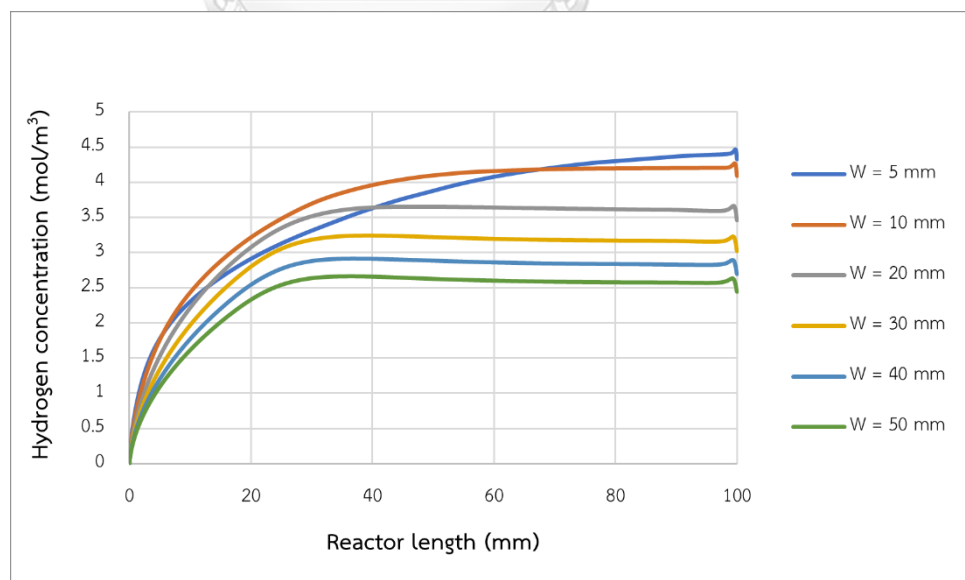
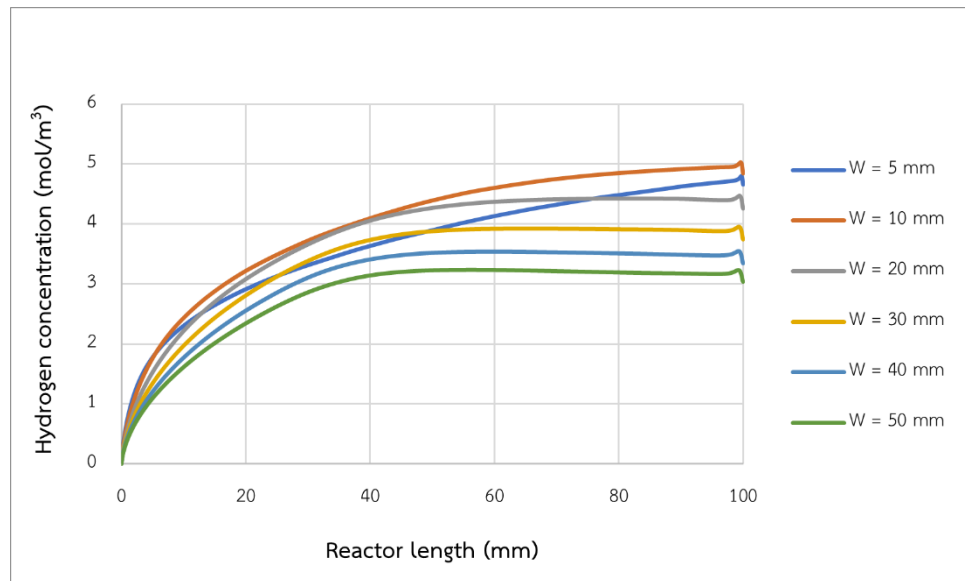**Figure 32.** Hydrogen concentration over reactor length at time = 120 second with varied catholyte channel width.

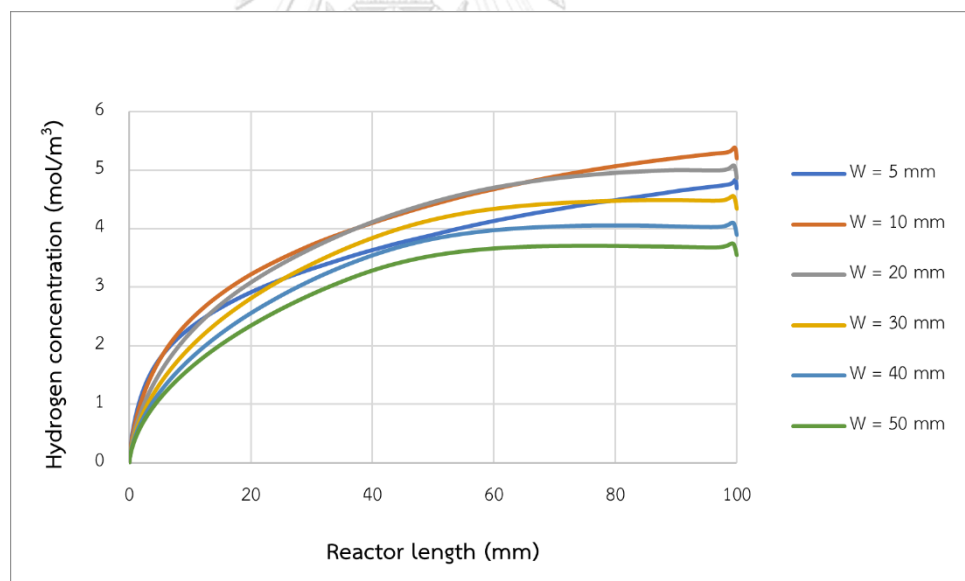**Figure 33.** Hydrogen concentration over reactor length at time = 180 second with varied catholyte channel width.

Figure 34. Hydrogen concentration over reactor length at time = 240 second with varied catholyte channel width.
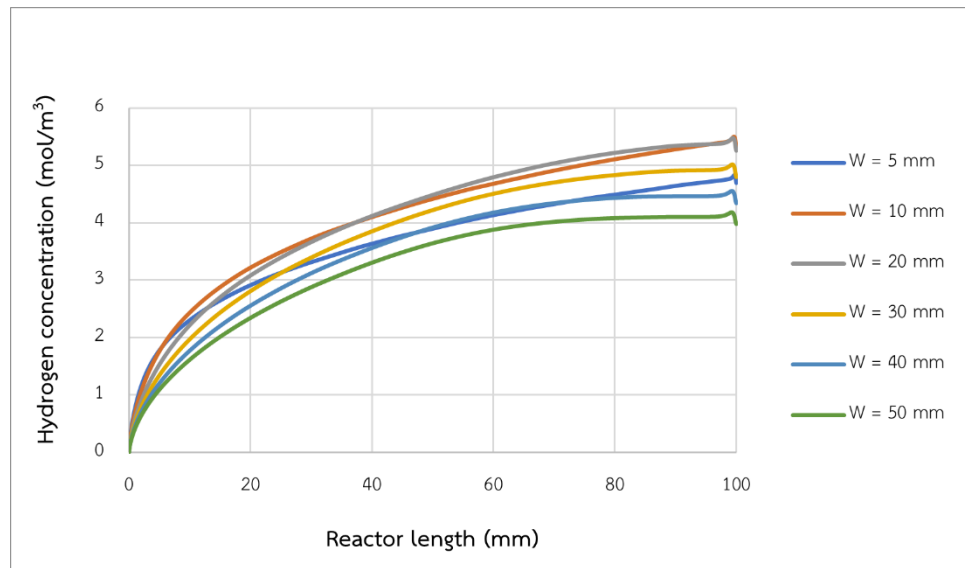
Figure 35. Hydrogen concentration over reactor length at time = 300 second with varied catholyte channel width.
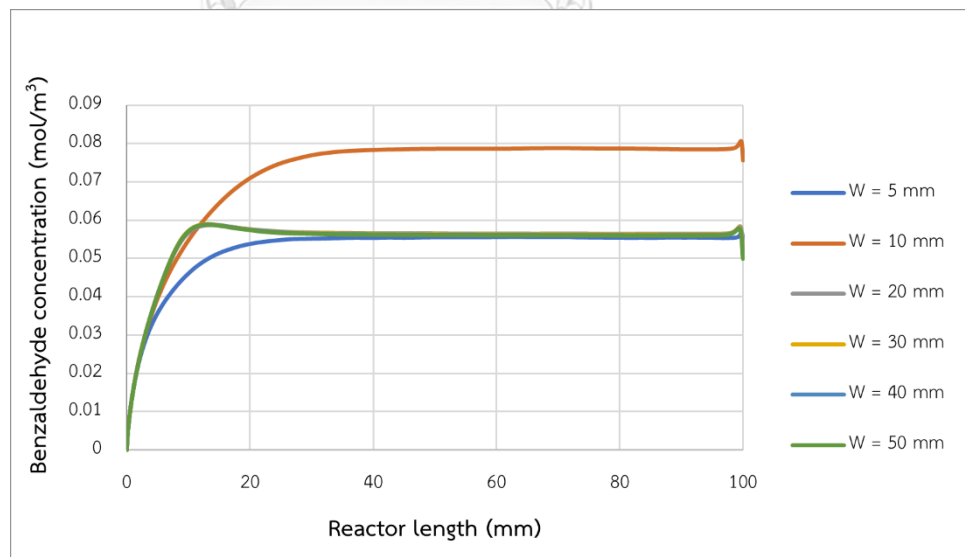
2. Benzaldehyde concentration

Figure 36. Benzaldehyde concentration over reactor length at time = 60 second with varied anolyte channel width.
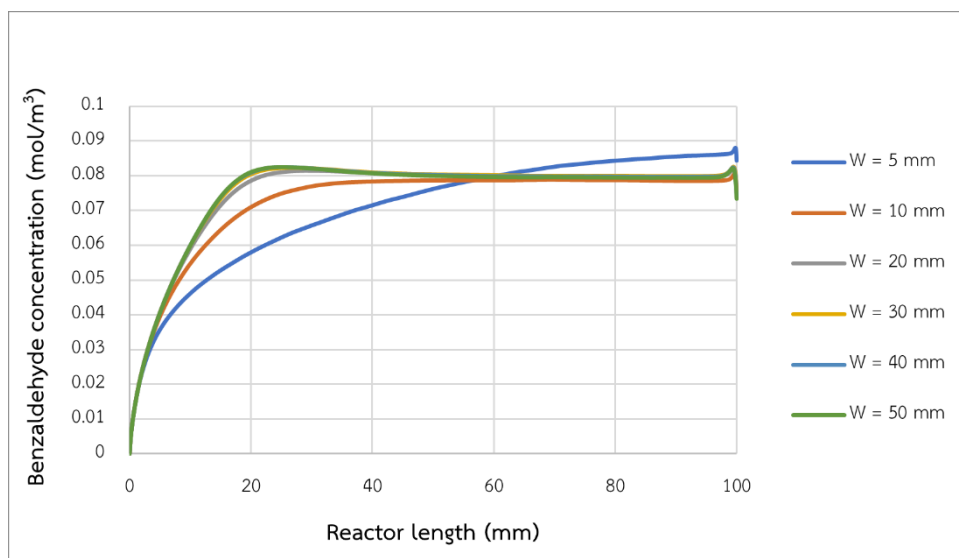
Figure 37. Benzaldehyde concentration over reactor length at time = 120 second with varied anolyte channel width.
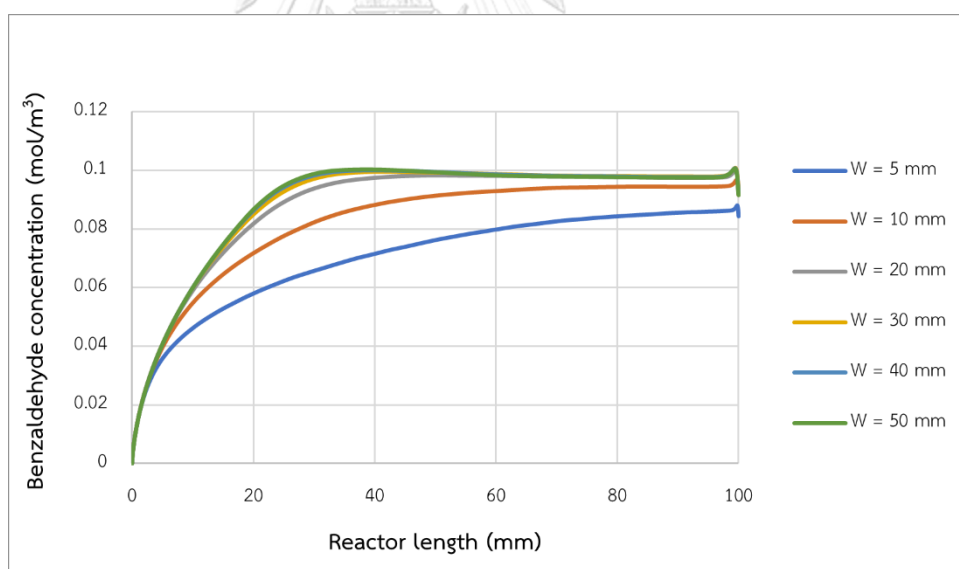

Figure 38. Benzaldehyde concentration over reactor length at time = 180 second with varied anolyte channel width.
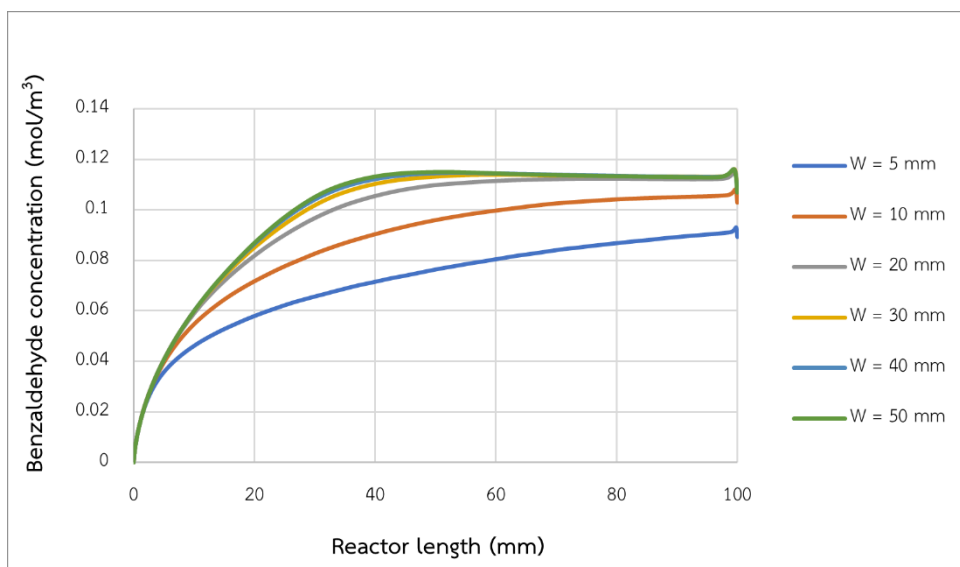
Figure 39. Benzaldehyde concentration over reactor length at time = 240 second with varied anolyte channel width.
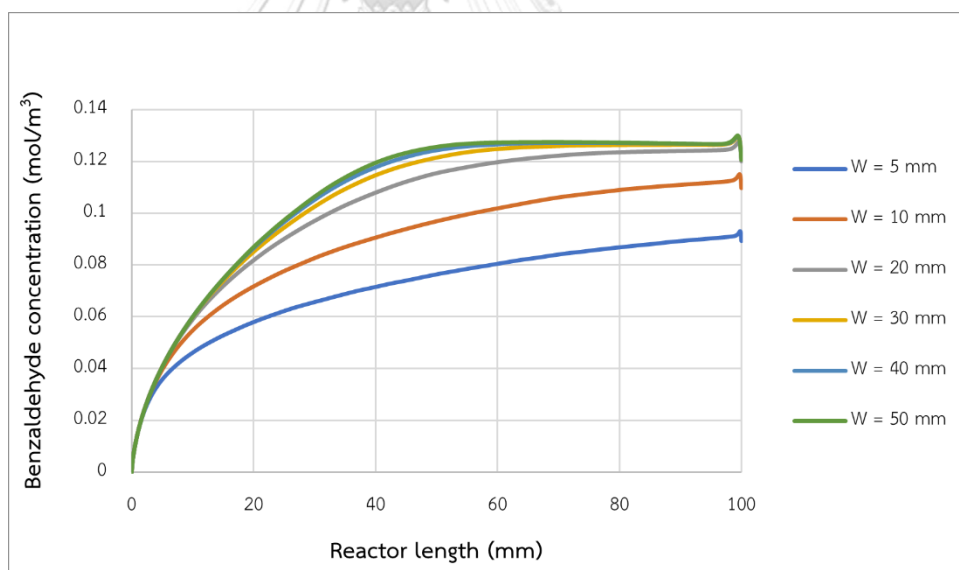

Figure 40. Benzaldehyde concentration over reactor length at time = 300 second with varied anolyte channel width.
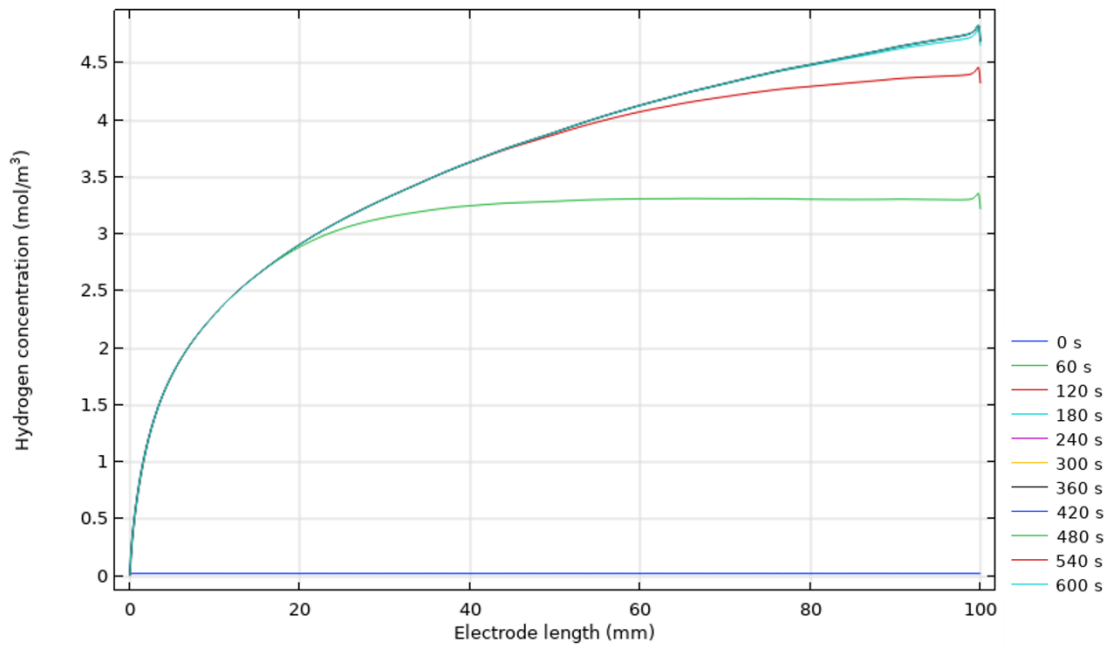
Figure 41. Hydrogen concentration over electrode length with varied time 0 to 600 second.
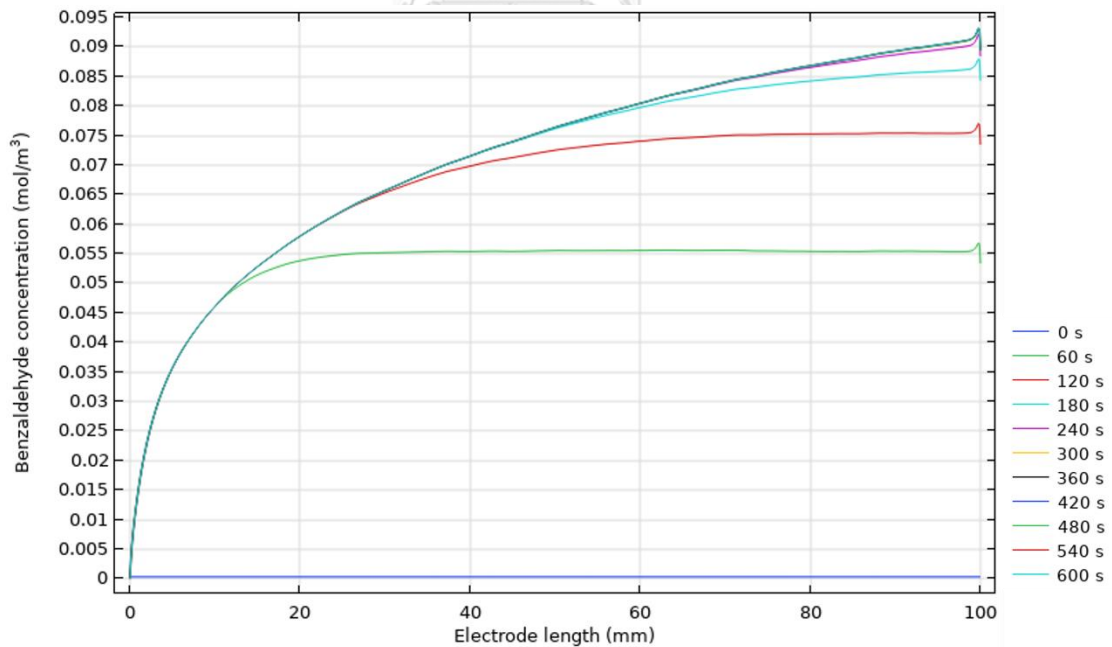

Figure 42. Benzaldehyde concentration over electrode length with varied time 0 to 600 second.

REFERENCES

[1]   Z. Wu, J. Wang, Z. Zhou, and G. Zhao, "Highly selective aerobic oxidation of biomass alcohol to benzaldehyde by an in situ doped Au/TiO2 nanotube photonic crystal photoanode for simultaneous hydrogen production promotion," *J. Mater. Chem. A.,* vol. 5, no. 24, pp. 12407-12415, 2017, doi: 10.1039/c7ta03252h.

[2]   A. U. S. E. Information. "Biomass Explained." https://www.eia.gov/energyexplained/biomass/ (accessed 27 January, 2022).

[3]   Y. C. Wu, R. J. Song, and J. H. Li, "Recent advances in photoelectrochemical cells (PECs) for organic synthesis," *Org. Chem. Front.,* vol. 7, no. 14, pp. 1895-1902, 2020, doi: https://doi.org/10.1039/d0qo00486c.

[4]   K. Sivula and R. Van de Krol, "Semiconducting materials for photoelectrochemical energy conversion," *Nat. Rev. Mater.,* vol. 1, no. 2, 2016, doi: 10.1038/natrevmats.2015.10.

[5]   B. Michael T, Y. Xin, and K. S. Choi, "Alcohol oxidation as alternative anode reactions paired with (photo)electrochemical fuel production reactions," *Nat. Commun.,* vol. 11, no. 1, 2020, doi: doi: 10.1038/s41467-020-18461-1.

[6]   J. A. Young, "Benzaldehyde," *Journal of Chemical Education,* vol. 82, no. 12, p. 1770, 2005, doi: 10.1021/ed082p1770.

[7]   X. Bao *et al.,* "TiO2/Ti3C2 as an efficient photocatalyst for selective oxidation of benzyl alcohol to benzaldehyde," *Applied Catalysis B: Environmental,* vol. 286, 2021, doi: 10.1016/j.apcatb.2021.119885.

[8]   M. J. Ndolomingo, N. Bingwa, and R. Meijboom, "Review of supported metal nanoparticles: synthesis methodologies, advantages and application as catalysts," *Journal of Materials Science,* vol. 55, no. 15, pp. 6195-6241, 2020, doi: 10.1007/s10853-020-04415-x.

[9]   E. T. a. R. M. Dolf Gielen, *Hydrogen: a Renewable Energy Perspective*. The International Renewable Energy Agency (IRENA), 2019.

[10]   T. F. a. F. Partnership, *Hydrogen Production: Overview of Technology Options*.

Agency of the United States Government, 2009.

[11] I. E. Agency, *Hydroprocessing of Heavy Oils and Residua*. Stedi Média, 2007.

[12] R. Krol, "Principles of Photoelectrochemical Cells," in *Photoelectrochemical Hydrogen Production*, (Electronic Materials: Science & Technology, 2012, ch. Chapter 2, pp. 13-67.

[13] C. Carver, Z. Ulissi, C. K. Ong, S. Dennison, G. H. Kelsall, and K. Hellgardt, "Modelling and development of photoelectrochemical reactor for H2 production," *International Journal of Hydrogen Energy,* vol. 37, no. 3, pp. 2911-2923, 2012, doi: 10.1016/j.ijhydene.2011.07.012.

[14] S. Schunemann, M. van Gastel, and H. Tuysuz, "A CsPbBr3 /TiO2 Composite for Visible-Light-Driven Photocatalytic Benzyl Alcohol Oxidation," *ChemSusChem,* vol. 11, no. 13, pp. 2057-2061, Jul 11 2018, doi: 10.1002/cssc.201800679.

[15] C. Xu *et al.*, "Ti3C2/TiO2 nanowires with excellent photocatalytic performance for selective oxidation of aromatic alcohols to aldehydes," *Journal of Catalysis,* vol. 383, pp. 1-12, 2020, doi: 10.1016/j.jcat.2020.01.001.

[16] Z. Zhou, Y.-N. Xie, W. Zhu, H. Zhao, N. Yang, and G. Zhao, "Selective photoelectrocatalytic tuning of benzyl alcohol to benzaldehyde for enhanced hydrogen production," *Applied Catalysis B: Environmental,* vol. 286, 2021, doi: 10.1016/j.apcatb.2020.119868.

[17] F. Farivar, "CFD simulation and development of an improved photoelectrochemical reactor for H 2 production," *Int. J. Hydrog.,* vol. 41, no. 2, pp. 882-888, 2016, doi: 10.1016/j.ijhydene.2015.11.045.

[18] F. N. Njoka, M. A. Ahmed, and S. Ookawara, "Design of a Novel Photoelectrochemical Reactor for Hydrogen Production," presented at the Energy and Sustainability VII, 2017.

[19] K. R. Applin and A. C. Lasaga, "The determination of SO42-, NaSO4-, and MgSO40 tracer diffusion coefficients and their application to diagenetic flux calculations," *Geochimica et Cosmochimica Acta,* vol. 48, no. 10, pp. 2151-2162, 1984, doi: 10.1016/0016-7037(84)90395-8.

[20] D. G. L. a. J. Goldik, "Diffusion and Ion Association in Concentrated Solutions of Aqueous Lithium, Sodium, and Potassium Sulfates," *Journal of Solution*

Chemistry, vol. 30, no. 2, pp. 103-118, 2001, doi: 10.1023/A:1005296425604.

[21] D. Y. Voropaeva, S. A. Novikova, T. L. Kulova, and A. B. Yaroslavtsev, "Solvation and sodium conductivity of nonaqueous polymer electrolytes based on Nafion-117 membranes and polar aprotic solvents," *Solid State Ion.,* vol. 324, pp. 28-32, 2018, doi: https://doi.org/10.1016/j.ssi.2018.06.002.

[22] A. Bally, "Electronic properties of nano-crystalline titanium dioxide thin films," 2094, Department of physics, FÉLÉRALE SCHOOL OF POLYTECHNICS DE LAUSANNE, Lausanne, 1999.

[23] "Solar Spectral Irradiance: Air Mass 1.5 n.d." http://rredc.nrel.gov/solar/spectra/am1.5/ (accessed March 20, 2022).

[24] N. Francis, O. Shinichi, and A. Mahmoud, "Influence of design and operating conditions on the performance of tandem photoelectrochemical reactors," *Int. J. Hydrog.,* vol. 43, pp. 1285-1302, 2017, doi: https://doi.org/10.1016/j.ijhydene.2017.11.168. Elsevier Ltd.

[25] K. Sivula and M. Grätzel, "CHAPTER 4 Tandem Photoelectrochemical Cells for Water Splitting," in *Photoelectrochemical Water Splitting: Materials, Processes and Architectures*: The Royal Society of Chemistry, 2013, pp. 83-108.

[26] G. S. Towler, *Chemical Engineering Design Principles, Practice and Economics of Plant and Process Design*. 30 Corporate Drive, Suite 400, Burlington, MA 01803, USA: Butterworth-Heinemann of Elsevier, 2008, p. 1266.

[27] A. Z. I.M. Abdulagatov, N.D. Azizov, "Viscosity of aqueous Na2SO4 solutions at temperatures from 298 to 573K and at pressures up to 40MPa," *Fluid Phase Equilibria,* vol. 227, no. 1, pp. 57-70, 2005, doi: 10.1016/j.fluid.2004.10.028.

VITA

NAME	Thorfhan Hanamorn
DATE OF BIRTH	15 September 1996
PLACE OF BIRTH	Uttaradit
HOME ADDRESS	196 Moo 1, Thasak, Phichai, Uttaradit, 53220